NKS-413
ISBN 978-87-7893-502-1

Development of a hybrid neutron transport solver in 2 energy groups – final report

Huaiqian Yi[1]
Christophe Demazière[1]
Paolo Vinai[1]
Jaakko Leppänen[2]

[1]Chalmers University of Technology, Sweden

[2]Technical Research Centre of Finland (VTT)

December 2018

Abstract

This project investigates the feasibility of performing reactor physics calculations for nuclear cores using a hybrid neutron transport methodology, by combining deterministic and probabilistic modelling techniques. In the presented implementation, a deterministic response matrix method was developed in Matlab. The necessary probabilities appearing in the response matrix method were estimated in advance using a probabilistic solver – the Monte Carlo code Serpent2. Ultimately, the hybrid framework will combine the advantages of the deterministic approach (fast running calculations) with the ones of the probabilistic approach (high flexibility in modelling any geometry and high accuracy). In the response matrix method, two grids are used: one fine grid for estimating the scalar neutron flux and a coarse grid for computing the neutron currents on this grid. In this second phase of the project, the framework was verified and new procedures to estimate the required probabilities were developed. Several two-dimensional test cases were then developed for benchmarking the computation of such probabilities and for benchmarking the response matrix framework itself. Compared to the earlier phase of the project, the framework now provides very good results, with a deviation of the dominant eigenvalue smaller than typically 50 pcm. Concerning the spatial distribution of the flux, some acceptable agreement was also obtained, with relative deviations generally smaller than 5%. In some cases, though, higher discrepancies were noticed. Additional investigations are necessary to identify the root cause of the larger observed deviations in such cases, in order to further increase the fidelity of the simulations.

Key words

nuclear reactor calculations, neutron transport, deterministic methods, probabilistic methods, hybrid methods

NKS-413
ISBN 978-87-7893-502-1
Electronic report, December 2018
NKS Secretariat
P.O. Box 49
DK - 4000 Roskilde, Denmark
Phone +45 4677 4041
www.nks.org
e-mail nks@nks.org

Development of a hybrid neutron transport solver in 2 energy groups

Final Report from the NKS-R HYBRID activity

(Contract: AFT/NKS-R(17)120/8)

Huaiqian Yi[1]
Christophe Demazière[1]
Paolo Vinai[1]
Jaakko Leppänen[2]

[1]Chalmers University of Technology, Department of Physics, Division of Subatomic and Plasma Physics, SE-412 96 Gothenburg, Sweden
[2]Technical Research Centre of Finland (VTT), P.O. Box 1000, FI-02044 VTT, Finland

Table of contents

Acknowledgements

NKS conveys its gratitude to all organizations and persons who by means of financial support or contributions in kind have made the work presented in this report possible.

Disclaimer

1 Introduction

The modelling of neutron transport problems for radiation transport purposes and nuclear reactor systems has long been divided into two types of approaches: the deterministic approach and the probabilistic approach.

In the deterministic approach, the neutron transport equation is solved explicitly after reducing the complexity of the task at hand (typically using space-homogenization, energy-condensation, and angular discretization techniques) (Demazière, 2013). The problem is first solved in a very small part of the computational domain using proper boundary conditions, and the solution then computed is used for transforming the problem into a problem encompassing a larger computational domain, at the expense of a simplification of the true complexity of the system. Typically, three to four of such "bottom-up" simplifications are used to model a full reactor core. Nevertheless, the validity of the approximations used in each of the computational steps are never corrected by the results of the calculations performed at the following computational step when a better (i.e. taking a larger computational domain into account) solution has been computed. Such methods are fast-running methods originally developed when the computing resources were limited.

In the probabilistic approach, also referred to as Monte Carlo, no equation as such is solved. Rather, the probability of occurrence of a nuclear reaction/process of a given type on a given species at a given energy for a given incoming particle (which can still exist after the nuclear interaction) is used to sample neutron life histories throughout the system (Lux and Koblinger, 1991). Using a very large number of such histories, the true behaviour of neutrons in the system can be reproduced. Due to the size and complexity of the systems usually modelled, Monte Carlo techniques are extremely expensive computing techniques, originally used for reference and shielding calculations.

With the development of cheap computing resources, both the deterministic approach and the probabilistic approach are currently being used on massively parallel clusters to circumvent the limitations mentioned above. In the deterministic case, the process of averaging ("bottom-up") is now being complemented by a de-averaging process ("top-down") in an interactive manner, so that a better modelling of the boundary conditions can be achieved using the information available from the coarser mesh. The modelling of full cores in one computational step only is also being attempted. In the probabilistic case, the use of large clusters allows modelling full reactor cores, and efforts are being pursued to include the effects induced by changes in the composition and/or density of the materials. Due to the complexity and level of details in the deterministic approach based on the averaging/de-averaging process, the deterministic route has become as computationally expensive as the probabilistic route for high-fidelity simulations.

The present project proposes to combine deterministic methods with probabilistic methods. The main advantage of such a *hybrid* route would be to lower the computational cost of the calculations (thanks to the use of deterministic methods) while still guaranteeing a high level of details and of reliability of the calculations (thanks to the use of probabilistic methods). A promising candidate for such a hybrid route is to use the so-called response matrix method, also known as the interface current method (Stacey, 2001; Stamm'ler & Abbate, 1983). This method is essentially a deterministic method, where two computational grids are used: one coarse grid for resolving the neutron currents between the thus-defined cells (assuming that

the neutron emission densities are known within the cells), and one finer grid for resolving within each cell the neutron emission densities (assuming that the neutron currents between cells are known). The solutions of the two grids are iteratively updated until convergence is reached. The application of such a method requires the prior determination of some specific probabilities within each cell. The prior determination of the necessary probabilities is a very difficult task, because of the three-dimensional nature of the problem at hand and of the possible geometrical complexity of the system.

The feasibility of a hybrid route was investigated in a previous NKS-funded project (contract AFT/NKS-R(16)120/7). This project concluded that (Carbol et al., 2017):

- It was possible to determine, using the Serpent2 Monte Carlo code (Leppänen et al., 2015), the collision probabilities required for applying the response matrix method.
- A hybrid framework relying on the response matrix method could be properly developed and used as a workbench for further development and testing.

Because of the large efforts developing a new computational framework represents and because such a developmental work is error-prone, it was decided in the first phase of the project to keep the system as simple as possible. With the objectives to lower the computational time and to have a tractable system, only two-dimensional systems representative of fuel assemblies having a regular lattice of fuel pins surrounded by coolant were thus considered during the feasibility study. This also means that the fine grid was chosen as made of a fuel pin and its associated coolant and the coarse grid was correspondingly made of the juxtaposition of such cells.

The feasibility study nevertheless also demonstrated that the implementation carried out for a simplified two-dimensional model of a BWR fuel assembly did not lead to physically-sound results for the infinite multiplication factor of the system. Likewise, the space-dependence of the neutron flux was somehow counter-intuitive. The reason of this unexpected behaviour had not been found at the time of the writing of the previous report (Carbol et al., 2017).

In the work performed for this contract period and reported hereafter, efforts were thus spent on verifying the developed framework, on correspondingly correcting possible errors, and on consolidating the framework. Two main actions were undertaken accordingly:

- A single fuel assembly in an infinite lattice was considered, for which the fine grid was chosen as made of a fuel pin and its associated coolant and the coarse grid was correspondingly made of the juxtaposition of such cells. A verification of the implementation earlier made was carried out, together with some improvements in the determination of the probabilities. An assessment of various ways of estimating the probabilities was then performed, and some corresponding benchmarking of the computed probabilities executed. The solution obtained from the hybrid route was also compared to the full Monte Carlo solution.
- The scalability of the hybrid method was then investigated. For that purpose, a new way to estimate the probabilities was developed, so that the associated computational cost could be lowered. Thereafter, the revised method was applied on a system of 2x2 fuel assemblies in an infinite lattice, for which the fine grid was either made of one fuel pin and its associated coolant or made of four fuel pins and their surrounding coolant regions. In both cases, the coarse grid was correspondingly made of the juxtaposition of such cells, and the hybrid solutions were compared to the full Monte Carlo solution.

This report is structured as follows. The essence of the hybrid solution strategy relying on the response matrix method is first recalled. The improvement of the hybrid method for test systems involving one fuel pin and one coolant region as fine meshes is then presented, together with the corresponding benchmark cases. Thereafter, the refinement of the method for test systems involving more regions as fine meshes is described, again together with a set of benchmark exercises. Finally, some conclusions and recommendations are given.

2 Reminder about the proposed hybrid method

As earlier indicated, the proposed hybrid method relies on the response matrix method or interface current method, which is a deterministic method (Stamm'ler and Abbate, 1983). Using standard notations in multi-energy group theory and using a classical transport correction of the total and scattering macroscopic cross-sections, the steady-state transport equation in its integral form written for the energy group g reads as:

$$\psi_g\left(\mathbf{r},\mathbf{\Omega}\right)=\int_0^{\infty}\exp\left[-\int_0^{s}\Sigma_{T,g}^{0}\left(\mathbf{r}-s'\mathbf{\Omega},E\right)ds'\right]\times q_g\left(\mathbf{r}-s\mathbf{\Omega},\mathbf{\Omega}\right)ds \tag{1}$$

where the emission density is given by:

$$q_g\left(\mathbf{r},\mathbf{\Omega}\right)=\frac{1}{4\pi}\sum_{g'=1}^{G}\left[\Sigma_{s0,g'\to g}^{0}\left(\mathbf{r}\right)+\chi_g\frac{\upsilon\Sigma_{f,g'}\left(\mathbf{r}\right)}{k_{eff}}\right]\phi_{g'}\left(\mathbf{r}\right) \tag{2}$$

Partitioning the volume V of the system into sub-volumes V_i, such that $V=\bigcup_i V_i$, and partitioning the outer surface S of the system into sub-surfaces S_a, such that $S=\bigcup_a S_a$, multiplying Eq. (1) by the transport-corrected total cross-section, assuming a homogeneous emission density on each sub-volume and integrating on one of the sub-volumes V_i lead to:

$$\Sigma_{T,g,j}^{0}\phi_{g,j}V_j=\sum_a S_a J_{in,g,a}P_{g,a\to j}+\sum_i V_i Q_{g,i}P_{g,i\to j} \tag{3}$$

where the emission density in energy group g and region i is given by:

$$Q_{g,i}=\frac{1}{4\pi}\sum_{g'\to 1}^{G}\left[\Sigma_{s0,g'\to g,i}^{0}+\frac{\chi_{g',i}\upsilon\Sigma_{f,g',i}}{k_{eff}}\right]\phi_{g',i} \tag{4}$$

Taking again Eq. (1) this time at the outer boundary of the system, multiplying this equation by $\left|\mathbf{\Omega}\cdot\mathbf{n}\right|$ where $\mathbf{n}$ is the outward unit vector normal to the considered surface, assuming a homogeneous emission density on each sub-volume and integrating on a given surface S and for solid angles such that $\mathbf{\Omega}\cdot\mathbf{n}>0$ lead to:

$$S_a J_{out,g,a}=\sum_b S_b J_{in,g,b}P_{g,b\to a}+\sum_i V_i Q_{i,g}P_{g,i\to a} \tag{5}$$

In the previous two equations, the different quantities have the following meaning:

- $J_{in,g,a}$ and $J_{out,g,a}$ represent the averaged incoming, outgoing respectively, neutron currents on the surface area S_a.
- $P_{g,i\to j}$ represents the probability for a neutron emitted in the volume V_i in an isotropic manner and having a given emission density to have its first collision in the volume V_j.
- $P_{g,a\to j}$ represents the probability for a neutron entering through the surface S_a to have its first collision in the volume V_j.
- $P_{g,i\to a}$ represents the probability for a neutron emitted in the volume V_i in an isotropic manner and having a given emission density to escape without interaction through the surface S_a .
- $P_{g,b\to a}$ represents the probability for a neutron entering through the surface S_b to escape without interaction through the surface S_a.

The above system of equations has nevertheless very limited practical usefulness since for a large system, the number of probabilities to be computed would be enormous. The essence of the response matrix method is thus to use two computational grids. If one considers that the system to be studied contains $I = 1,...,N$ sub-systems, each having respectively a volume V_I delimited by a surface S_I, Eqs. (3) and (5) can be written on each of the sub-systems as:

$$\Sigma^0_{T,g,j}\phi_{g,j}V_j = \sum_{a\in S_I} S_a J_{in,g,a,} P_{g,a\to j} + \sum_{i\in V_I} V_i Q_{g,i} P_{g,i\to j} \text{ for } j \in V_I \tag{6}$$

$$S_a J_{out,g,a} = \sum_{b\in S_I} S_b J_{in,g,b} P_{g,b\to a} + \sum_{i\in V_I} V_i Q_{g,i} P_{g,i\to a} \text{ for } a \in S_I \tag{7}$$

If $\mathbf{J}^I_{out}$ represents the vector having for components each of the currents $J_{out,a}$ on all sub-surfaces belonging the boundary of the sub-system I, if $\mathbf{J}^I_{in}$ represents the vector having for components each of the currents $J_{in,a}$ on all sub-surfaces belonging to the boundary of the sub-system I, and if $\mathbf{J}^I_{source}$ represents the vector having for components the contribution to the current $J_{out,a}$ due to volumetric sources inside the sub-system I, the set of equations (6) can be recast in the following vector equation:

$$\mathbf{J}^I_{out} = \mathbf{R}^I \times \mathbf{J}^I_{in} + \mathbf{J}^I_{source} \tag{8}$$

where $\mathbf{R}^I$ is referred to as the response matrix for the sub-system I. Such a vector equation can be written for any sub-system I of the computational domain, and thus one can write:

$$\mathbf{J}_{out} = \mathbf{R} \times \mathbf{J}_{in} + \mathbf{J}_{source} \tag{9}$$

for the entire system being modelled. In this equation, $\mathbf{R}$ is referred to as the response matrix for the entire system. Since the outgoing current from a given sub-system is equal to the incoming current to its neighbouring sub-system, a topographical relationship exists between $\mathbf{J}_{in}$ and $\mathbf{J}_{out}$ which can be generically written as:

$$\mathbf{J}_{in} = \mathbf{P} \times \mathbf{J}_{out} \tag{10}$$

where $\mathbf{P}$ is a matrix defined for the entire system being considered. Combining Eqs. (9) and (10) leads to:

$$\mathbf{J}_{in} = \mathbf{P} \times \mathbf{R} \times \mathbf{J}_{in} + \mathbf{P} \times \mathbf{J}_{source} \tag{11}$$

This equation represents the *global* problem, i.e. the problem defined for the entire computational domain. Likewise, Eq. (6) can also be recast into the following vector equation:

$$\phi^{I} = \mathbf{S}^{I} \times \mathbf{J}_{in}^{I} + \phi_{source}^{I} \tag{12}$$

This equation represents the *local* problem, i.e. the problem defined for the sub-system I. This means that two different computational grids are used: a coarse grid to resolve the neutron currents and the associated coupling between the coarse regions, and a fine grid to resolve the neutron flux within each region, as illustrated in Fig. 1.

The probabilities $P_{g,a\to j}$, $P_{g,i\to j}$, $P_{g,b\to a}$, and $P_{g,i\to a}$ need to be calculated prior to the application of the response matrix method. Nevertheless, compared to the original formulation of the transport problem as given by Eqs. (3) and (5), only probabilities within each sub-system need to be evaluated when two computational grids (i.e. a global problem and a local problem) are used. Once the different probabilities have been evaluated, the solution procedure goes as follows. From a known distribution of the emission densities for the entire computational domain, the global problem is solved, i.e. the neutron currents between each sub-system are computed using Eq. (11). Once the currents have been determined, the local problem is solved for each of the sub-systems, i.e. the scalar neutron fluxes within each sub-system are determined using Eq. (12). The calculated neutron fluxes within each sub-system are then used to calculate an updated distribution of the emission densities for the next inner iteration.

As in the previous contract period, the Monte Carlo tool Serpent2 was used to evaluate the probabilities within each of the sub-systems for each of the local problems (Leppänen et al., 2015).

The update of the effective multiplication factor of the system is calculated on-the-fly by the deterministic solution procedure, using a classical power iteration method (Stamm'ler and Abbate, 1983):

$$k^{(p)} = k^{(p-1)} \frac{\Phi^{(p-1)} \cdot \Phi^{(p)}}{\Phi^{(p-1)} \cdot \Phi^{(p-1)}} \tag{13}$$

where p represents the outer iteration number, k is the dominant eigenvalue of the system, and the vector ϕ represents a vector having as elements the flux values in each of the modelled regions.

In the hybrid implementation, the computational burden of estimating the probabilities are left to the Monte Carlo tool. Because of the small sizes of the sub-systems, estimating such probabilities is comparatively much faster than determining the probabilities for the entire system. Furthermore, the estimation of the probabilities represents independent tasks, and parallel computing techniques could be used to distribute the required calculations when large scale systems would have to be considered.

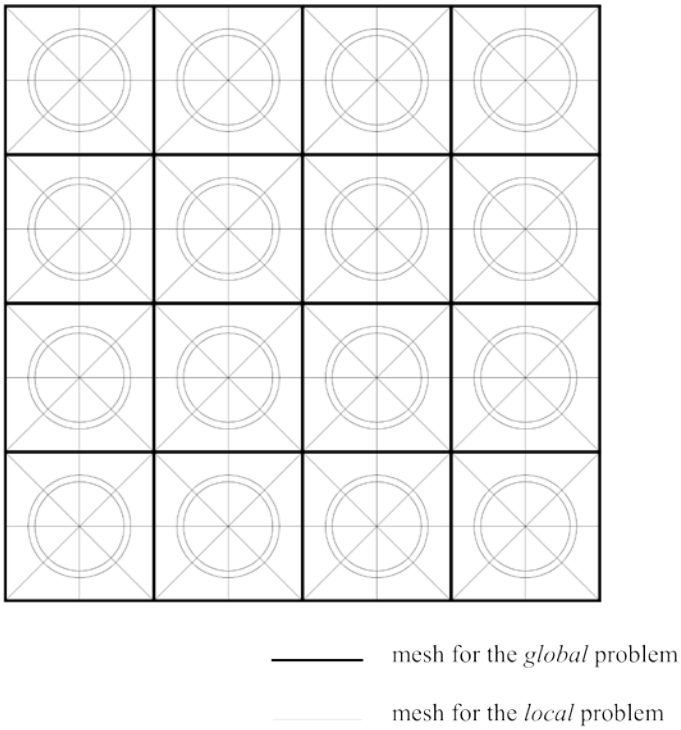

Fig. 1 Example of a coarse and a fine mesh computational grids that could be used in the response matrix method.

3 Improvement of the hybrid method for local problems representing 1x1 fuel pin cell

In the first phase of this contract period, the hybrid framework previously developed was carefully checked. Special attention was paid to the estimation of the probabilities.

3.1 Description of the test system

The problem considered hereafter is representative of a two-dimensional axial cross-section of a fuel assembly. The system is made of a lattice of 10x10 fuel pins. The local mesh is made of two regions per fuel cell: a fuel region and a moderator region. The global mesh is thus made of the juxtaposition of such elementary fuel cells to create the 10x10 fuel pin lattice.

For the sake of simplicity, the water gaps, cladding and fuel box were disregarded, resulting in a regular lattice of fuel pins for the system considered, as illustrated in Fig. 2. The fuel pin pitch is $p = 1.295\ \mathrm{cm}$ and the fuel rod radius is $R_f = 0.4335\ \mathrm{cm}$. The fuel density is set to 10.424 g/cm^3. The moderator, assumed to be made of H_2O, has a density of 0.444 g/cm^3.

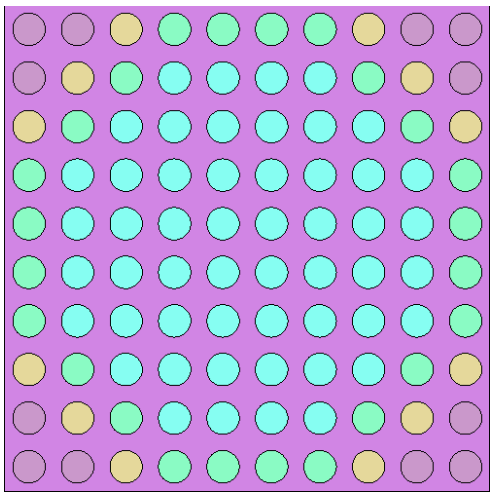

$$\begin{bmatrix} 2 & 2 & 3 & 5 & 5 & 5 & 5 & 3 & 2 & 2 \\ 2 & 3 & 5 & 6 & 6 & 6 & 6 & 5 & 3 & 2 \\ 3 & 5 & 6 & 6 & 6 & 6 & 6 & 6 & 5 & 3 \\ 5 & 6 & 6 & 6 & 6 & 6 & 6 & 6 & 6 & 5 \\ 5 & 6 & 6 & 6 & 6 & 6 & 6 & 6 & 6 & 5 \\ 5 & 6 & 6 & 6 & 6 & 6 & 6 & 6 & 6 & 5 \\ 5 & 6 & 6 & 6 & 6 & 6 & 6 & 6 & 6 & 5 \\ 3 & 5 & 6 & 6 & 6 & 6 & 6 & 6 & 5 & 3 \\ 2 & 3 & 5 & 6 & 6 & 6 & 6 & 5 & 3 & 2 \\ 2 & 2 & 3 & 5 & 5 & 5 & 5 & 3 & 2 & 2 \end{bmatrix}$$

Fuel pin number	U-235 [1]	U-238 [1]	O-16 [1]
1	0.015867	0.86563	0.1185
2	0.018512	0.86299	0.1185
3	0.022919	0.85858	0.1185
4	0.026445	0.85505	0.1185
5	0.029971	0.85153	0.1185
6	0.032615	0.84888	0.1185

Fig. 2 Radial layout of the modelled fuel assembly (left) with the corresponding fuel pin types (right) and their respective compositions (mass fractions of materials in the fuel pins).

In the work reported in this report, the implementation of the hybrid method and all tests were performed using a two-group formalism. The required macroscopic cross-sections are thus the total cross-section $\Sigma_{T,g}$, the group-to-group isotropic scattering cross-section $\Sigma_{s0,g\to g'}$ and the fission "production" cross-section $\upsilon\Sigma_{f,g}$ for each of the $g = 1,2$ and $g' = 1,2$ energy groups. All fission neutrons are assumed to be emitted in the fast energy group only. The two-group cross-sections are generated from Serpent2 for the fuel and moderator regions, respectively, for all fuel pin types.

For the scattering cross-sections, two kinds of scattering matrices are given by Serpent2. The first kind is the scattering matrix where the $(n,2n')$, $(n,3n')$, etc. reactions are not included. The second kind is the scattering matrix where such reactions are accounted for as:

$$\Sigma_{s0,g\to g'} = \Sigma_{(n,n')0,g\to g'} + 2\Sigma_{(n,2n')0,g\to g'} + 3\Sigma_{(n,3n')0,g\to g'} + 4\Sigma_{(n,3n')0,g\to g'} \qquad (14)$$

Since most notably the $\left(n,2n'\right)$ reactions have an appreciable effect in light water reactors, the use of the scattering matrix including the $\left(n,2n'\right)$, $\left(n,3n'\right)$, etc. reactions in the hybrid method was tested. The absorption cross-section, although not used in the hybrid method, would be adjusted according to:

$$\Sigma_{a,g}{}' = \Sigma_{a,g} - \sum_{g'=1}^{2}\Sigma_{\left(n,2n'\right)0,g\to g'} - 2\sum_{g'=1}^{2}\Sigma_{\left(n,3n'\right)0,g\to g'} - 3\sum_{g'=1}^{2}\Sigma_{\left(n,4n'\right)0,g\to g'} \quad (15)$$

so that the total cross-section $\Sigma_{T,g}$ is conserved.

Irrespective of the inclusion or non-inclusion of inelastic scattering reactions, only isotropic scattering was considered in the cross-section used in the hybrid framework.

The Serpent2 calculations, in addition to provide the necessary cross-section data and probabilities, are also used in the following as a reference solution for the spatial distribution of the two-energy group neutron flux in each of the regions defined in the local problems and for the effective multiplication factor of the system. In order to obtain results with a high accuracy, 10000 source neutrons per cycle, 5000 cycles with 500 inactive cycles were used for the Serpent2 calculations. The corresponding running time was approximately 80 min.

3.2 Procedures for estimating the required probabilities

Compared to the first contract period, the procedure for estimating the probabilities required in the hybrid method was revised.

The determination of the probabilities is carried out on the local mesh, as defined in Fig. 3.

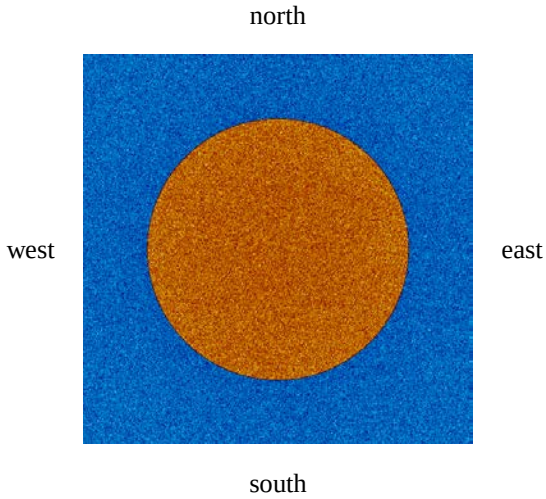

Fig. 3 Representation of an elementary subsystem (fuel region in red and coolant region in blue). Each subsystem has 4 surfaces defining its outer boundary (north, east, south, and west).

The probabilities for neutrons emitted in the fuel and moderator, respectively are calculated separately using two separate input files. The seed (i.e. random numbers) is nevertheless set to be the same in both cases. The reason for separating the two sets of calculations is twofold. First, for each set of probabilities, the number of detectors used is large. Second, the sequence for defining the detectors in the input might sometimes have an impact of the results, since the

determination of the probabilities requires defining many "detectors" in Serpent2 to keep track of the neutrons.

Neutrons emitted from the fuel

Neutrons emitted in the fuel will either first interact in the fuel, in the moderator or escape through any of the four surfaces. With the following definitions:

$N_{fuel,g}$: Neutrons in group g emitted from fuel

$R_{fuel\to fuel,g}$: Neutrons in group g emitted from fuel to first interact in fuel

$R_{fuel\to \mathrm{mod},g}$: Neutrons in group g emitted from fuel to first interact in moderator

$R_{fuel\to w,g}$: Neutrons in group g emitted from fuel to escape through west surface

$R_{fuel\to e,g}$: Neutrons in group g emitted from fuel to escape through east surface

$R_{fuel\to s,g}$: Neutrons in group g emitted from fuel to escape through south surface

$R_{fuel\to n,g}$: Neutrons in group g emitted from fuel to escape through north surface

the following relationship should be fulfilled:

$$N_{fuel,g} = R_{fuel\to fuel,g} + R_{fuel\to \mathrm{mod},g} + R_{fuel\to w,g} + R_{fuel\to e,g} + R_{fuel\to s,g} + R_{fuel\to n,g} \qquad (16)$$

The probabilities corresponding to each of the terms on the right-hand side of Eq. (16) are obtained by dividing each term by the left-hand side of Eq. (16).

In order to determine the first term on the right-hand side of Eq. (16), an additional equation is nevertheless required. The neutrons having their first interaction in the fuel region can originate from the fuel, the moderator or any of the four surfaces. Using the following definitions

$R_{fuel,total,g}$: Neutrons in group g having any kind of interaction in the fuel

$R_{\mathrm{mod}\to fuel,g}$: Neutrons in group g emitted from moderator to first interact in fuel

$R_{w\to fuel,g}$: Neutrons in group g entering from west surface to first interact in fuel

$R_{e\to fuel,g}$: Neutrons in group g entering from east surface to first interact in fuel

$R_{s\to fuel,g}$: Neutrons in group g entering from south surface to first interact in fuel

$R_{n\to fuel,g}$: Neutrons in group g entering from north surface to first interact in fuel

the following balance equation can be written:

$$R_{fuel\to fuel,g} = R_{fuel,total,g} - R_{\mathrm{mod}\to fuel,g} - R_{w\to fuel,g} - R_{e\to fuel,g} - R_{s\to fuel,g} - R_{n\to fuel,g} \qquad (17)$$

The following procedure is then used to determine the different terms in Eq. (17):

- The total number of any kind of interaction occurring in the fuel region is directly determined in Serpent2.
- For the surface-to-fuel reactions, taking one surface as an example, a flag, number 10 for instance, is set if the neutron enters the surface. The surface flag number 10 is removed if the neutron travels to any other surface or has interaction in the moderator. Then the neutrons with flag 10 still set represent the neutrons interacting in the fuel. Such neutrons are thus counted, and the flag 10 is thereafter removed.
- For the moderator-to-fuel reactions, since no fission occurs in the moderator region, one considers that neutrons emitted from the moderator can only be due to scattering. In Serpent2, reactions of the type $\left(n,2n'\right)$, $\left(n,3n'\right)$, etc. are also modelled. Nevertheless,

such reactions are highly unlikely in the moderator and can thus be neglected – this assumption was verified. A flag 31 is set if a neutron is scattered in the moderator. The flag is removed if this neutron escapes through any of the surfaces. Then the neutrons with flag 31 still set represent the neutrons interacting in the fuel. Such neutrons are thus counted, and the flag 31 is thereafter removed.

To determine the second to the sixth terms on the right-hand side of Eq. (16), the following method is used. A surface detector is set at the cylindrical fuel boundary to detect neutrons entering the fuel region through its surface, and flag 40 is set if this occurs. Flag 40 is removed if the neutron has thereafter an interaction in the fuel. For neutrons leaving the fuel region, a surface current detector for outgoing current at the cylindrical fuel boundary is set. This detector is scored if and only if flag 40 is not set, and flag 41 is set if the outgoing current detector is scored. By doing this, neutrons entering the fuel region and crossing the fuel region without interacting can be excluded from the outgoing current from the fuel region. If neutrons have flag 41 set and then interact in the moderator, they represent neutrons that are emitted from fuel and that first interact in the moderator. Such neutrons are thus counted, and flag 41 is thereafter removed. If neutrons have flag 41 set and escape through any of the surfaces, they represent neutrons that are emitted from the fuel and that escape through any of the surfaces. Such neutrons are thus counted, and flag 41 is thereafter removed.

The above procedure is repeated for both the fast and thermal energy groups and for each fuel pin type in a single run. Each run takes approximately 30 min without using any parallel computing option.

Neutrons emitted from the moderator

As earlier indicated, the set of probabilities for neutrons emitted from the moderator is calculated via a different input file, so that the detectors used to estimate the neutrons emitted from the fuel cannot erroneously influence the tracking of the neutrons in the moderator region.

Similar to the counting of neutrons emitted from the fuel region, a balance equation for the moderator region is established as:

$$N_{mod,g} = R_{mod\to mod,g} + R_{mod\to fuel,g} + R_{mod\to w,g} + R_{mod\to e,g} + R_{mod\to s,g} + R_{mod\to n,g} \qquad (18)$$

with the different terms defined as:

$N_{mod,g}$: Neutrons in group g emitted from moderator

$R_{mod\to mod,g}$: Neutrons in group g emitted from moderator to first interact in moderator

$R_{mod\to fuel,g}$: Neutrons in group g emitted from moderator to first interact in fuel

$R_{mod\to w,g}$: Neutrons in group g emitted from moderator to escape through west surface

$R_{mod\to e,g}$: Neutrons in group g emitted from moderator to escape through east surface

$R_{mod\to s,g}$: Neutrons in group g emitted from moderator to escape through south surface

$R_{mod\to n,g}$: Neutrons in group g emitted from moderator to escape through north surface

In order to determine the first term on the right-hand side of Eq. (18), an additional equation is nevertheless required. The neutrons having their first interaction in the moderator region can

originate from the moderator, the fuel or any of the four surfaces. Using the following definitions:

$R_{mod,total,g}$: Neutrons in group g having any kind of interaction in the moderator

$R_{fuel\to mod,g}$: Neutrons in group g emitted from moderator to first interact in moderator

$R_{w\to mod,g}$: Neutrons in group g entering from west surface to first interact in moderator

$R_{e\to mod,g}$: Neutrons in group g entering from east surface to first interact in moderator

$R_{s\to mod,g}$: Neutrons in group g entering from south surface to first interact in moderator

$R_{n\to mod,g}$: Neutrons in group g entering from north surface to first interact in moderator

the following balance equation can be written:

$$R_{mod\to mod,g} = R_{mod,total,g} - R_{fuel\to mod,g} - R_{w\to mod,g} - R_{e\to mod,g} - R_{s\to mod,g} - R_{n\to mod,g} \quad (19)$$

The following procedure is then used to determine the different terms in Eq. (19):

- The total number of any kind of interaction occurring in the moderator region is directly determined in Serpent2.
- For the surface-to-moderator reactions, a similar implementation as the one used for the surface-to-fuel reactions is followed. Taking one surface as an example, a flag, number 10 for instance, is set if the neutron enters the surface. The surface flag number 10 is removed if the neutron travels to any other surface or has interaction in the fuel. Then the neutrons with flag 10 still set represent the neutrons interacting in the moderator. Such neutrons are thus counted, and the flag 10 is thereafter removed.
- For fuel-to-moderator reactions, a similar implementation as the one used for the fuel region is also followed. A surface detector is set at the cylindrical fuel boundary to detect neutrons entering the fuel through its surface, and flag 40 is set if this occurs. Flag 40 is removed if the neutron has thereafter an interaction in the fuel. For neutrons leaving the fuel region, a surface current detector for outgoing current at the cylindrical fuel boundary is set. This detector is scored if and only if flag 40 is not set, and flag 41 is set if the outgoing current detector is scored. By doing this, neutrons entering the fuel region and crossing the fuel region without interacting can be excluded from the outgoing current from the fuel region. If neutrons have flag 41 set and then escape through any of the surfaces, flag 41 is removed. If neutrons have flag 41 set and interacts in the moderator, they represent neutrons that are emitted from the fuel and that first interact in the moderator. Such neutrons are thus counted, and flag 41 is thereafter removed.

To determine the second to the sixth term on the right-hand side of Eq. (18), it is again assumed that the neutrons emitted from the moderator region are only due to scattering and that reactions of the type $\left(n,2n'\right)$, $\left(n,3n'\right)$, etc. can be neglected. A flag 31 is set if a neutron is scattered in the moderator. Neutrons with flag 31 set and having any kind of interaction in the fuel represent neutrons that are emitted from moderator and that first interact in the fuel region. Such neutrons are thus counted, and flag 31 is removed. Neutrons with flag 31 set and escaping through any of the surfaces represent neutrons that are emitted from the moderator and that directly escape through any of the outer surfaces. Such neutrons are also counted, and flag 31 is thereafter removed.

The above procedure is repeated for both the fast and thermal energy groups and for each fuel pin type in a single run. Each run takes approximately 32 min without using any parallel computing option.

It should also be pointed out that the method for calculating the probabilities, as described above, is not general, since the system being considered is only allowed to contain one fuel region and one moderator region surrounding the fuel region. Furthermore, the input cards are quite lengthy due to the relatively large number of detectors used, which in itself results in many neutrons being tracked in the Monte Carlo calculations and leads to a higher computing cost.

With the procedure highlighted above, the probabilities were evaluated. Table 1 gives the probabilities for neutrons emitted from the fuel, Table 2 gives the probabilities for neutrons emitted from the moderator and Table 3 gives the probabilities for neutrons entering through any of outer boundaries of the pin system. In the last case, the probabilities are only given for one pin type (pin type #1).

Table 1 Probabilities for neutrons emitted from the fuel region.

	Pin	$P_{fuel \to fuel}$	$P_{fuel \to mod}$	$P_{fuel \to w}$	$P_{fuel \to e}$	$P_{fuel \to s}$	$P_{fuel \to n}$	Sum
Fast	1	0.20675	0.12699	0.16645	0.16669	0.16651	0.16662	1.00000
	2	0.20698	0.12708	0.16644	0.16656	0.16647	0.16647	1.00000
	3	0.20736	0.12658	0.16633	0.16648	0.16643	0.16681	1.00000
	4	0.20713	0.12619	0.16668	0.16651	0.16668	0.16680	1.00000
	5	0.20743	0.12617	0.16680	0.16648	0.16655	0.16657	1.00000
	6	0.20753	0.12569	0.16681	0.16675	0.16678	0.16643	1.00000
Thermal	1	0.24482	0.27405	0.12030	0.12063	0.12016	0.12004	1.00000
	2	0.25166	0.26911	0.12029	0.11986	0.11956	0.11951	1.00000
	3	0.26138	0.26339	0.11859	0.11903	0.11871	0.11890	1.00000
	4	0.26781	0.25791	0.11875	0.11906	0.11828	0.11819	1.00000
	5	0.27508	0.25369	0.11730	0.11790	0.11756	0.11847	1.00000
	6	0.28124	0.24980	0.11717	0.11782	0.11714	0.11683	1.00000

Table 2 Probabilities for neutrons emitted from the moderator.

	Pin	$P_{mod \to mod}$	$P_{mod \to fuel}$	$P_{mod \to w}$	$P_{mod \to e}$	$P_{mod \to s}$	$P_{mod \to n}$	Sum
Fast	1	0.22830	0.08148	0.17248	0.17259	0.17270	0.17245	1.00000
	2	0.22816	0.08162	0.17275	0.17260	0.17255	0.17231	1.00000
	3	0.22797	0.08224	0.17240	0.17245	0.17252	0.17242	1.00000
	4	0.22775	0.08220	0.17262	0.17245	0.17245	0.17253	1.00000
	5	0.22735	0.08233	0.17257	0.17257	0.17252	0.17266	1.00000
	6	0.22750	0.08268	0.17255	0.17266	0.17215	0.17246	1.00000
Thermal	1	0.38662	0.07995	0.13336	0.13337	0.13335	0.13334	1.00000
	2	0.38373	0.08242	0.13337	0.13356	0.13361	0.13331	1.00000
	3	0.37992	0.08584	0.13339	0.13377	0.13334	0.13374	1.00000
	4	0.37693	0.08868	0.13334	0.13375	0.13346	0.13383	1.00000
	5	0.37431	0.09133	0.13347	0.13355	0.13353	0.13381	1.00000
	6	0.37207	0.09313	0.13363	0.13386	0.13384	0.13347	1.00000

Table 3 Probabilities for neutrons emitted from surfaces.

	To → / From↓	fuel	moderator	west	east	south	north	sum
fast	west	0.12558	0.23916	0	0.21601	0.20964	0.20961	1.00000
	east	0.12554	0.23923	0.21588	0	0.20974	0.20960	1.00000
	south	0.12531	0.23914	0.20983	0.20954	0	0.21618	1.00000
	north	0.12536	0.23931	0.20944	0.20962	0.21627	0	1.00000
thermal	west	0.12233	0.50323	0	0.10782	0.13320	0.13342	1.00000
	east	0.12195	0.50284	0.10789	0	0.13352	0.13380	1.00000
	south	0.12187	0.50316	0.13356	0.13361	0	0.10780	1.00000
	north	0.12199	0.50299	0.13338	0.13354	0.10810	0	1.00000

As can be seen from the results given in Table 1 and Table 2, for each type of fuel pin and for each energy group, the region-to-surface probabilities are different depending on the surface being considered. Similarly, Table 3 shows that the surface-to-fuel probabilities for each type of fuel pin and each energy group are different depending on the emitting surface being considered. Due to the symmetry of the system, the region-to-surface and the surface-to-region probabilities should be identical, respectively, irrespective of the surface being considered. This can be achieved by improving the accuracy of the Monte Carlo calculations, i.e. by simulating more cycles and/or adding more source neutrons. The number of source neutrons per cycle, the number of cycles and the number of skipped cycles were thus doubled compared to the previous calculations reported in Table 1, Table 2 and Table 3. The results corresponding to the increased accuracy of the Monte Carlo simulations are reported in Table 4. In this table, only the probabilities for neutrons emitted from the fuel region for the first pin type are given. The difference between the largest and smallest values of the fuel-to-surface probabilities were, in the previous calculations, 0.00024 and 0.00059 for fast and thermal groups, respectively (see Table 1). The improved accuracy in the Monte Carlo simulations results in differences of 0.0018 and 0.00028, for the fast and thermal groups, respectively (see Table 4). A significant improvement is seen in the thermal group. The differences cannot, nevertheless, be fully eliminated.

Table 4 Probabilities for neutrons emitted from the fuel region for increased accuracy of the Monte Carlo simulations.

	Pin	$P_{fuel \to fuel}$	$P_{fuel \to mod}$	$P_{fuel \to w}$	$P_{fuel \to e}$	$P_{fuel \to s}$	$P_{fuel \to n}$	Sum
Fast	1	0.20700	0.12729	0.16650	0.16645	0.16632	0.16645	1.00000
Thermal	1	0.24523	0.27327	0.12029	0.12057	0.12030	0.12034	1.00000

3.3 Benchmarking of the computed probabilities

The probabilities estimated according to the procedure explained in Section 4.1 were benchmarked against probabilities evaluated in a deterministic sense using Carlvik's method (Carlvik, 1965).

In this method, the squared-shape of the outer boundary of the system being modelled is replaced by a circular outer boundary using the Wigner-Seitz cell approximation, according to which the outer radius of the moderator region is given as:

$$R_m = p\Big/\sqrt{\pi} \tag{20}$$

White boundary conditions are then applied on the outer surface and the albedo is set to unity. The deterministic probabilities are calculated as detailed hereafter.

First, the region-to-region probabilities $P_{i\to j,g}$ are estimated according to the following expression:

$$P_{i\to j,g} = \delta_{ij} + \frac{2}{\Sigma^0_{T,i,g} A_i}\left[S_{i,j} - S_{i-1,j} - S_{i,j-1} + S_{i-1,j-1}\right] \tag{21}$$

where

$$S_{i,j} = \int_0^{R_i}\left[\mathrm{Ki}_3\left(\tau^+_{i,j}\right) - \mathrm{Ki}_3\left(\tau^-_{i,j}\right)\right]dy \tag{22}$$

In the equations above, isotropic emissions in the laboratory reference system are assumed. The indexes i and j denote the region where neutrons are emitted and the region where those neutrons first interact, respectively, and A_i is the area of the corresponding emitting region i. In the present case, the fuel region is labelled as region 1, whereas the moderator region is labelled as region 2. With the numbering chosen, Eq. (21) is only valid for $j \geq i$. In Eq. (22), $\tau^{\pm}_{i,j}$ represents the optical path associated to the distance $T^{\pm}_{i,j}$ represented in Fig. 4, and Ki_3 is the third-order Bickley function, defined as:

$$\mathrm{Ki}_3\left(x\right) = \int_0^{\pi/2}\left(\cos\theta\right)^2 \exp\left(-\frac{x}{\cos\theta}\right)d\theta \tag{23}$$

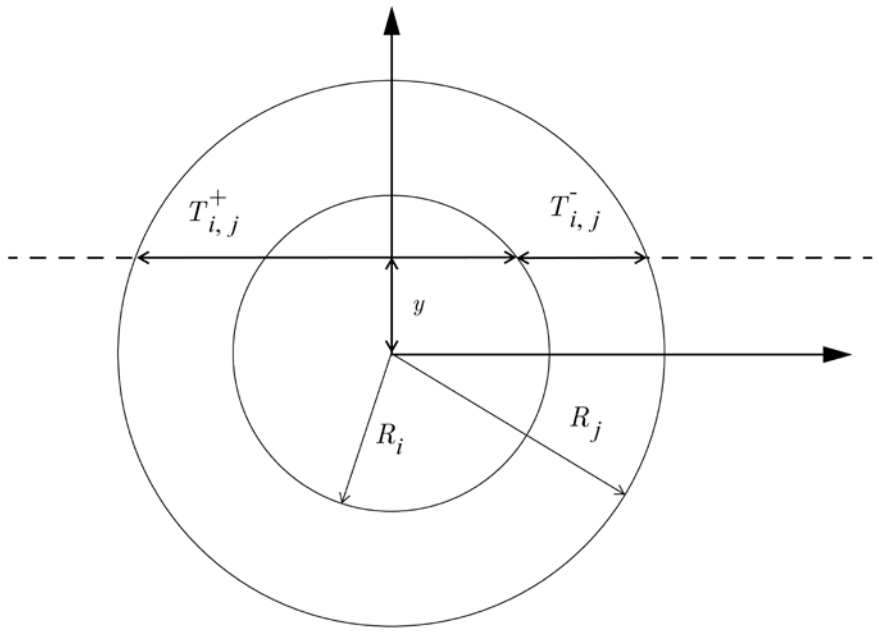

Fig. 4 Representation of the two-region system being modelled. The plot shows the distances $T^{\pm}_{i,j}$ along a line being away from the origin by a distance y.

Since Eq. (21) is only valid for $j \geq i$, the following reciprocity relationship is used to estimate all remaining region-to-region probabilities:

$$\Sigma^{0}_{T,i,g} A_i P_{i\to j,g} = \Sigma^{0}_{T,j,g} A_j P_{j\to i,g} \tag{24}$$

Then the region-to-outer moderator surface probabilities are calculated using the following complementarity relationship:

$$P_{i\to S,g} = 1 - \sum_{j} P_{i\to j,g} \tag{25}$$

Thereafter, the surface-to-region probabilities, using the reciprocity of the probabilities, are calculated as:

$$P_{S\to i,g} = \frac{4A_i\Sigma^{0}_{T,i,g}}{2\pi R_m} P_{i\to S,g} \tag{26}$$

Finally, the surface-to-surface probability is given, using again the property of complementarity of the probabilities, as:

$$P_{S\to S,g} = 1 - \sum_{i} P_{S\to i,g} \tag{27}$$

As can be seen above, the region-to-surface, surface-to-region and surface-to-surface probabilities are given for one single outer boundary of the moderator region assumed to be circular. In the actual geometry, the outer boundary is made of four distinct parts representing a square, as depicted in Fig. 3. Even in a circularly-equivalent formulation, a post-processing of the probabilities determined above is thus required, so that probabilities with respect to the

circularly-equivalent west, east, south and north faces of each elementary fuel cell can be recovered.

Due to the symmetry of the problem, one has for the region-to-surface probabilities:

$$P_{i\to w,g} = P_{i\to e,g} = P_{i\to s,g} = P_{i\to n,g} = \frac{P_{i\to S,g}}{4} \tag{28}$$

and for the surface-to-region probabilities:

$$P_{w\to i,g} = P_{e\to i,g} = P_{s\to i,g} = P_{n\to i,g} = P_{S\to i,g} \tag{29}$$

It should be noticed that in Eq. (28), the region-to-surface probabilities are obtained by dividing $P_{i\to S,g}$ by four, since a neutron has a one fourth probability to reach each of the circularly-equivalent surfaces. In Eq. (29), on the other hand, the surface-to-region probabilities are all equal to $P_{S\to i,g}$, since the probabilities are estimated by renormalizing the interaction rates in the region i with the surface emission density, furthermore assumed to be uniform and isotropic on the emitting surfaces.

For the surface-to-surface probabilities, there is no simple way to recover the surface-to-surface probabilities for each of the four circularly-equivalent west, east, south and north surfaces. The surface-to-same surface probability should nevertheless be set to zero, since a neutron emitted from a surface cannot cross the same surface without first interacting. For the surfaces not corresponding to the emitting surface, the probabilities estimated from the Monte Carlo procedure highlighted in Section 4.1 are used to estimate, in an approximative manner, a corresponding weighting factor. More specifically, the relative weight of a surface-to-another surface probability from the Monte Carlo procedure is used to determine the corresponding fraction in $P_{S\to S,g}$. For instance, $P_{w\to e,g}$ is calculated according to:

$$P_{w\to e,g} = \frac{P^{MC}_{w\to e,g}}{P^{MC}_{w\to e,g} + P^{MC}_{w\to s,g} + P^{MC}_{w\to n,g}} P_{S\to S,g} \tag{30}$$

where the superscript MC denotes the probabilities estimated from the Monte Carlo procedure detailed in Section 4.1.

The probabilities estimated according to the procedure detailed above are given in Table 5 for neutrons emitted from the fuel, in Table 6 for neutrons emitted from the moderator, and in Table 7 for neutrons emitted from the surfaces. For the last case, the probabilities are only given for one fuel pin type (fuel pin type #1).

Table 5 Probabilities for neutrons emitted from the fuel region.

	Pin	$P_{fuel\to fuel}$	$P_{fuel\to mod}$	$P_{fuel\to w}$	$P_{fuel\to e}$	$P_{fuel\to s}$	$P_{fuel\to n}$	Sum
Fast	1	0.19289	0.13563	0.16787	0.16787	0.16787	0.16787	1.00000
	2	0.19307	0.13535	0.16790	0.16790	0.16790	0.16790	1.00000
	3	0.19342	0.13487	0.16793	0.16793	0.16793	0.16793	1.00000
	4	0.19358	0.13454	0.16797	0.16797	0.16797	0.16797	1.00000
	5	0.19382	0.13427	0.16798	0.16798	0.16798	0.16798	1.00000
	6	0.19398	0.13406	0.16799	0.16799	0.16799	0.16799	1.00000
Thermal	1	0.24570	0.28912	0.11629	0.11629	0.11629	0.11629	1.00000
	2	0.25215	0.28476	0.11577	0.11577	0.11577	0.11577	1.00000
	3	0.26238	0.27805	0.11489	0.11489	0.11489	0.11489	1.00000
	4	0.27014	0.27312	0.11418	0.11418	0.11418	0.11418	1.00000
	5	0.27743	0.26864	0.11348	0.11348	0.11348	0.11348	1.00000
	6	0.28292	0.26533	0.11294	0.11294	0.11294	0.11294	1.00000

Table 6 Probabilities for neutrons emitted from the moderator region.

	Pin	$P_{mod\to mod}$	$P_{mod\to fuel}$	$P_{mod\to w}$	$P_{mod\to e}$	$P_{mod\to s}$	$P_{mod\to n}$	Sum
Fast	1	0.18389	0.07665	0.18486	0.18486	0.18486	0.18486	1.00000
	2	0.18356	0.07673	0.18493	0.18493	0.18493	0.18493	1.00000
	3	0.18303	0.07689	0.18502	0.18502	0.18502	0.18502	1.00000
	4	0.18264	0.07698	0.18510	0.18510	0.18510	0.18510	1.00000
	5	0.18235	0.07708	0.18514	0.18514	0.18514	0.18514	1.00000
	6	0.18211	0.07715	0.18519	0.18519	0.18519	0.18519	1.00000
Thermal	1	0.38186	0.08066	0.13437	0.13437	0.13437	0.13437	1.00000
	2	0.37912	0.08281	0.13452	0.13452	0.13452	0.13452	1.00000
	3	0.37495	0.08620	0.13471	0.13471	0.13471	0.13471	1.00000
	4	0.37192	0.08876	0.13483	0.13483	0.13483	0.13483	1.00000
	5	0.36922	0.09114	0.13491	0.13491	0.13491	0.13491	1.00000
	6	0.36724	0.09294	0.13496	0.13496	0.13496	0.13496	1.00000

Table 7 Probabilities for neutrons emitted from surfaces.

	To → / From↓	fuel	moderator	west	east	south	north	sum
fast	west	0.14613	0.28478	0	0.19351	0.18781	0.18777	1.00000
	east	0.14613	0.28478	0.19341	0	0.18790	0.18778	1.00000
	south	0.14613	0.28478	0.18789	0.18763	0	0.19357	1.00000
	north	0.14613	0.28478	0.18760	0.18776	0.19372	0	1.00000
thermal	west	0.13714	0.56797	0	0.08491	0.10490	0.10507	1.00000
	east	0.13714	0.56797	0.08479	0	0.10494	0.10516	1.00000
	south	0.13714	0.56797	0.10503	0.10507	0	0.08478	1.00000
	north	0.13714	0.56797	0.10488	0.10501	0.08500	0	1.00000

The deviation between the probabilities P estimated as above and the ones P^{MC} estimated from the Monte Carlo procedure as detailed in Section 4.1 is characterized in relative terms (%) using the following expression:

$$\Delta P = 100\frac{P - P^{MC}}{P^{MC}} \tag{31}$$

The relative deviations are summarized in Table 8 for neutrons emitted from the fuel, in Table 9 for neutrons emitted from the moderator, and in Table 10 for neutrons emitted from the surfaces. For the last case, the probabilities are only given for one fuel pin type (fuel pin type #1).

Table 8 Relative difference for the probabilities for neutrons emitted from the fuel region.

	Pin	$\Delta P_{fuel\to fuel}$	$\Delta P_{fuel\to mod}$	$\Delta P_{fuel\to w}$	$\Delta P_{fuel\to e}$	$\Delta P_{fuel\to s}$	$\Delta P_{fuel\to n}$
Fast	1	-6.7%	6.8%	0.9%	0.7%	0.8%	0.8%
	2	-6.7%	6.5%	0.9%	0.8%	0.9%	0.9%
	3	-6.7%	6.5%	1.0%	0.9%	0.9%	0.7%
	4	-6.5%	6.6%	0.8%	0.9%	0.8%	0.7%
	5	-6.6%	6.4%	0.7%	0.9%	0.9%	0.8%
	6	-6.5%	6.7%	0.7%	0.7%	0.7%	0.9%
Thermal	1	0.4%	5.5%	-3.3%	-3.6%	-3.2%	-3.1%
	2	0.2%	5.8%	-3.8%	-3.4%	-3.2%	-3.1%
	3	0.4%	5.6%	-3.1%	-3.5%	-3.2%	-3.4%
	4	0.9%	5.9%	-3.8%	-4.1%	-3.5%	-3.4%
	5	0.9%	5.9%	-3.3%	-3.7%	-3.5%	-4.2%
	6	0.6%	6.2%	-3.6%	-4.1%	-3.6%	-3.3%

Table 9 Relative difference for the probabilities for neutrons emitted from the moderator region.

	Pin	$\Delta P_{mod\to mod}$	$\Delta P_{mod\to fuel}$	$\Delta P_{mod\to w}$	$\Delta P_{mod\to e}$	$\Delta P_{mod\to s}$	$\Delta P_{mod\to n}$
Fast	1	-19.5%	-5.9%	7.2%	7.1%	7.0%	7.2%
	2	-19.5%	-6.0%	7.0%	7.1%	7.2%	7.3%
	3	-19.7%	-6.5%	7.3%	7.3%	7.2%	7.3%
	4	-19.8%	-6.4%	7.2%	7.3%	7.3%	7.3%
	5	-19.8%	-6.4%	7.3%	7.3%	7.3%	7.2%
	6	-20.0%	-6.7%	7.3%	7.3%	7.6%	7.4%
Thermal	1	-1.2%	0.9%	0.8%	0.7%	0.8%	0.8%
	2	-1.2%	0.5%	0.9%	0.7%	0.7%	0.9%
	3	-1.3%	0.4%	1.0%	0.7%	1.0%	0.7%
	4	-1.3%	0.1%	1.1%	0.8%	1.0%	0.7%
	5	-1.4%	-0.2%	1.1%	1.0%	1.0%	0.8%
	6	-1.3%	-0.2%	1.0%	0.8%	0.8%	1.1%

Table 10 Relative difference for the probabilities for neutrons emitted from surfaces.

	To → / From↓	fuel	moderator	west	east	south	north
fast	west	16.4%	19.1%	0.0%	-10.4%	-10.4%	-10.4%
	east	16.4%	19.0%	-10.4%	0.0%	-10.4%	-10.4%
	south	16.6%	19.1%	-10.5%	-10.5%	0.0%	-10.5%
	north	16.6%	19.0%	-10.4%	-10.4%	-10.4%	0.0%
thermal	west	12.1%	12.9%	0.0%	-21.2%	-21.2%	-21.2%
	east	12.5%	13.0%	-21.4%	0.0%	-21.4%	-21.4%
	south	12.5%	12.9%	-21.4%	-21.4%	0.0%	-21.4%
	north	12.4%	12.9%	-21.4%	-21.4%	-21.4%	0.0%

As compared with the probabilities estimated from the Monte Carlo procedure explained in Section 4.1, the following trends for the probabilities estimated in the procedure explained above are observed:

- $P_{mod \to mod}$ is underestimated for the fast neutrons.
- $P_{mod \to surface}$ are overestimated for the fast neutrons.
- $P_{surface \to mod}$ are overestimated for the fast neutrons.
- $P_{surface \to surface}$ are underestimated for both the fast and thermal neutrons.

The probabilities above also show somewhat larger discrepancies compared to the other probabilities. Since the surface-related probabilities and moderator-related probabilities heavily rely on the outer region and surface, which are modelled in a different manner between the Monte Carlo-based probabilities (see Section 4.1) and the ones estimated above, the possible influence of the modelling of the outer boundary onto the probabilities was examined.

There are several factors that might influence the observed discrepancies:

- The modelling of the entry of neutrons via the outer surface is assumed to be isotropic and uniform on the outer surface in the deterministic estimation of the probabilities, whereas there is no such any assumption in the Monte Carlo procedure for estimating the probabilities.
- The outer square-shaped boundary, which is correctly modelled in the Monte Carlo procedure, is replaced by an outer boundary having a circular shape in the deterministic evaluation of the probabilities.

Intuitively, it is thus expected that changing the size of the outer region only might lead to a significant variation of the discrepancies between the deterministic and Monte Carlo-based probabilities related to the outer surface and moderator region, without changing much the ones related to the fuel region.

The pin pitch p was thus increased and the different probabilities recomputed accordingly. These recalculations were only performed for the fuel pin type #1. The variations in relative differences as a function of the fuel pin pitch are given in Table 11 for neutrons emitted from the fuel region and in Table 12 for neutrons emitted from the moderator region. The relative

differences for the probabilities for neutrons emitted from surfaces are given in Table 13 for a fuel pin pitch of 1.8 cm and in Table 14 for a fuel pin pitch of 3.6 cm.

Table 11 Relative difference for the probabilities for neutrons emitted from the fuel region when changing the fuel pin pitch.

	Pin Pitch [cm]	$\Delta P_{fuel\to fuel}$	$\Delta P_{fuel\to mod}$	$\Delta P_{fuel\to w}$	$\Delta P_{fuel\to e}$	$\Delta P_{fuel\to s}$	$\Delta P_{fuel\to n}$
Fast	1.295	-6.7%	6.8%	0.9%	0.7%	0.8%	0.8%
	1.8	-3.2%	16.4%	-4.6%	-4.1%	-4.5%	-4.5%
	3.6	9.1%	44.2%	-31.8%	-32.3%	-31.9%	-31.8%
Thermal	1.295	0.4%	5.5%	-3.3%	-3.6%	-3.2%	-3.1%
	1.8	-2.1%	3.0%	-2.6%	-3.0%	-2.4%	-2.0%
	3.6	-3.0%	2.1%	-6.5%	-6.6%	-6.9%	-7.2%

Table 12 Relative difference for the probabilities for neutrons emitted from the moderator region when changing the fuel pin pitch.

	Pin Pitch [cm]	$\Delta P_{mod\to mod}$	$\Delta P_{mod\to fuel}$	$\Delta P_{mod\to w}$	$\Delta P_{mod\to e}$	$\Delta P_{mod\to s}$	$\Delta P_{mod\to n}$
Fast	1.295	-19.5%	-5.9%	7.2%	7.1%	7.0%	7.2%
	1.8	-16.6%	-3.3%	9.8%	10.0%	9.9%	10.0%
	3.6	-10.3%	3.3%	14.2%	14.1%	14.3%	14.1%
Thermal	1.295	-1.2%	0.9%	0.8%	0.7%	0.8%	0.8%
	1.8	-2.2%	1.9%	2.9%	2.8%	2.8%	2.8%
	3.6	-1.0%	6.5%	3.2%	3.1%	3.1%	3.2%

Table 13 Relative difference for the probabilities for neutrons emitted from surfaces and a fuel pin pitch of 1.8 cm.

	To → / From↓	fuel	moderator	west	east	south	north
fast	west	16.9%	24.2%	0.0%	-12.5%	-20.0%	-20.0%
	east	17.1%	24.2%	-12.6%	0.0%	-20.0%	-19.9%
	south	16.9%	24.3%	-20.0%	-20.2%	0.0%	-12.4%
	north	16.9%	24.2%	-20.1%	-20.1%	-12.3%	0.0%
thermal	west	12.8%	10.1%	0.0%	-2.6%	-38.6%	-38.3%
	east	12.4%	10.1%	-2.8%	0.0%	-38.4%	-38.4%
	south	12.4%	10.1%	-38.4%	-38.2%	0.0%	-2.8%
	north	13.0%	10.1%	-38.7%	-38.5%	-2.2%	0.0%

Table 14 Relative difference for the probabilities for neutrons emitted from surfaces and a fuel pin pitch of 3.6 cm.

	To → / From↓	fuel	moderator	west	east	south	north
fast	west	10.1%	29.1%	0.0%	-41.1%	-41.1%	-41.1%
	east	10.0%	29.1%	-41.2%	0.0%	-41.2%	-41.2%
	south	9.6%	29.2%	-41.2%	-41.2%	0.0%	-41.2%
	north	10.3%	29.0%	-41.1%	-41.1%	-41.1%	0.0%
thermal	west	11.5%	7.3%	0.0%	-60.8%	-60.8%	-60.8%
	east	11.0%	7.3%	-60.7%	0.0%	-60.7%	-60.7%
	south	11.3%	7.3%	-60.7%	-60.7%	0.0%	-60.7%
	north	10.9%	7.3%	-60.8%	-60.8%	-60.8%	0.0%

As can be seen in the tables above, the largest relative differences previously observed for the moderator-to-moderator probabilities are decreased with the fuel pin pitch is increasing. However, the relative differences for the moderator-to-surface and fuel-to-region or surface are increased with a larger fuel pin pitch. By comparing the probabilities for neutrons emitted from surfaces at the nominal fuel pin pitch (Table 10), at a fuel pin pitch of 1.8 cm (Table 13) and at a fuel pin pitch of 3.6 cm (Table 14), it can be seen that the relative differences for surface-to-moderator probabilities in the fast group and for the surface-to-surface probabilities increase, while the relative differences for the surface-to-moderator probabilities in the thermal group decrease.

Although the above trends might indicate that the reasons of the discrepancies are indeed related to the different modelling of the outer boundary and the emission of neutrons on those, more intricate inter-related phenomena prevent from drawing clear conclusions.

It should nevertheless be mentioned that, for the original fuel pin pitch, the probabilities evaluated in a deterministic manner and the ones estimated from Monte Carlo seem to qualitatively agree with each other. This demonstrates that the probabilities estimated from the Monte Carlo procedure developed in this project seem to be "sufficiently well" evaluated, despite some differences noted with the deterministically-based probabilities determined using different approximations.

3.4 Flux and eigenvalue calculations

With the probabilities evaluated from Monte Carlo (see Section 4.2) or in a "deterministic" sense (see Section 4.3), the hybrid framework was used to estimate the spatial distribution of the fast and thermal neutron flux throughout the system, as well as the eigenvalue. Those calculations are also directly compared with the pure Monte Carlo solution. In the hybrid framework, the convergence criteria for both the flux and eigenvalue was set to 10^{-10} in relative difference between two consecutive iterations.

The results in term of eigenvalue are summarized in Table 15. Two types of calculations were performed, either not including the $\left(n,2n'\right)$, $\left(n,3n'\right)$, etc. reactions in the scattering matrices used in the hybrid method or by including such reactions. As can be seen in this table,

including the $\left(n,2n'\right)$, $\left(n,3n'\right)$, etc. reactions in the scattering matrices used in the hybrid method leads to a much better agreement with the reference Monte Carlo solution. In addition, using the probabilities evaluated from Monte Carlo leads to a difference between the hybrid solution and the reference Monte Carlo solution of only +5 pcm. This demonstrates that the hybrid framework is properly implemented and that the probabilities determined from Monte Carlo method explained in Section 4.2 are correctly estimated. The correct implementation of the hybrid framework is further demonstrated by the fact that using the "deterministic" probabilities leads to a difference between the hybrid solution and the reference Monte Carlo solution of only +109 pcm.

Table 15 Evaluation of the dominant eigenvalue of the modelled system for the reference Monte Carlo solution and the hybrid solutions.

Case	Scattering matrices not including the $\left(n,2n'\right)$, $\left(n,3n'\right)$, etc. reactions in the hybrid calculations		Scattering matrices including the $\left(n,2n'\right)$, $\left(n,3n'\right)$, etc. reactions in the hybrid calculations	
	k_{eff}	$\Delta\rho$ [pcm]	k_{eff}	$\Delta\rho$ [pcm]
Reference Monte Carlo solution	1.27003±0.00007	Reference	1.27003±0.00007	Reference
Hybrid solution with Monte Carlo probabilities	1.26744	-259	1.27008	5
Hybrid solution with "deterministic" probabilities	1.26849	-154	1.27112	109

The spatial distribution of the fast and thermal fluxes along the diagonal of the lattice are given for the reference Monte Carlo solution and the hybrid solution using the Monte Carlo probabilities in Fig. 5. Both solutions are renormalized as:

$$\phi_g^{normalized}\left(\mathbf{r}\right)=\frac{\phi_g\left(\mathbf{r}\right)}{\sum_{g'=1}^{2}\upsilon\Sigma_{f,g'}\left(\mathbf{r}\right)\phi_{g'}\left(\mathbf{r}\right)} \tag{32}$$

The flux obtained from Serpent2 was calculated using lattice detectors for both the fuel and moderator regions. The lattice detector creates a bin for each lattice position (100 in the current case), for both the fuel and moderator regions at each lattice position. As an illustrative example, a sample lattice detector used for estimating the fast flux integrated on the moderator region can be defined, for every lattice position, as:

det 1 dm cool dl 10 de 2gfast dv 1.0866 (33)

For a detector defined by Eq. (12), the flux is integrated in the moderator region for every lattice position and for the fast group. In order to have similar space-homogenized fluxes in each moderator region, the integrated flux is normalized, using the "dv" option, by the area occupied by each moderator region, which is 1.0866 cm^2 in the present case and in the two-

dimensional representation chosen for the modelled system. Similarly, the integrated flux in the fuel region is normalized by 0.5904, which is the area in cm^2 occupied by each fuel region.

As can be seen in Fig. 5, the shape of both the thermal and fast fluxes is correctly reproduced by the hybrid method, as compared to the reference Monte Carlo solution. The agreement is particularly good for the thermal group. For the fast group, the overall buckling of the flux is different.

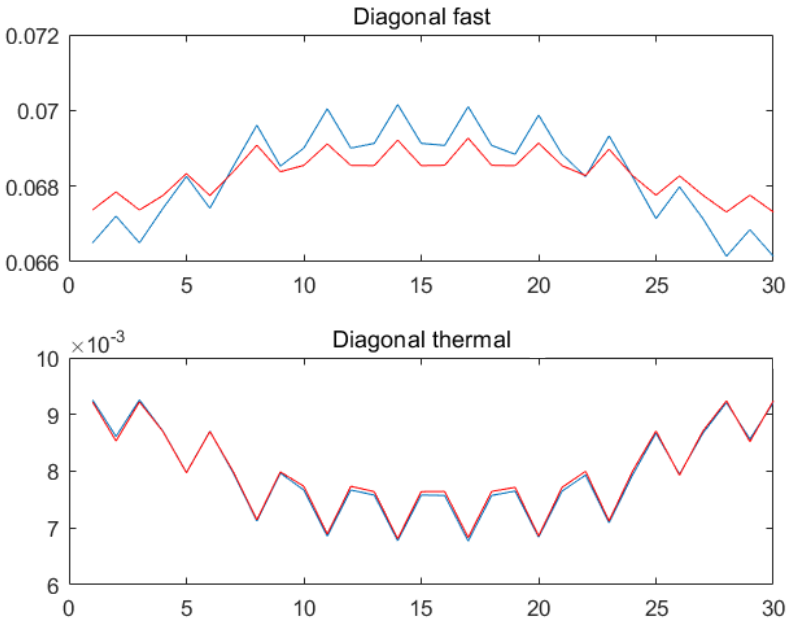

Fig. 5 Spatial distribution of the fast and thermal neutron flux along the diagonal of the lattice for the reference Monte Carlo solution (in red) and for the hybrid solution using the Monte Carlo probabilities (in blue).

4 Extension of the hybrid method for local problems representing 2x2 fuel pin cells

4.1 Procedure for estimating the required probabilities

When the local problem contains more than one fuel pin cell, the number of probabilities to be determined by the Monte Carlo code Serpent2 significantly increases. In order to decrease the computational time associated with the computation of those probabilities, the method used to determine those is revised.

Within each cell, the probabilities to be determined are the ones related to the neutrons emitted from the fuel, the neutrons emitted from the moderator, and the neutrons entering the cell through the outer surfaces, respectively. Only the methods for the first two types are modified and reported hereafter. The methods for the probabilities related to the neutrons entering through the outer surfaces are identical to the ones earlier described in Section 4.2.

For the sake of simplicity and of comparison with the method presented in Section 4.2, the revised version of the computation of the probabilities is described hereafter for a 1x1 fuel pin cell system.

Neutrons emitted from the moderator

Denoting as:

$$
\begin{aligned}
&N_{mod,g} : \text{ Neutrons in group } g \text{ emitted from moderator} \\
&R_{mod\to mod,g} : \text{ Neutrons in group } g \text{ emitted from moderator to first interact in moderator} \\
&R_{mod\to fuel,g} : \text{ Neutrons in group } g \text{ emitted from moderator to first interact in fuel} \\
&R_{mod\to surfaces,g} : \text{ Neutrons in group } g \text{ emitted from moderator to escape through surfaces}
\end{aligned}
\tag{34}
$$

the following relationship should be fulfilled:

$$N_{mod,g} = R_{mod\to mod,g} + R_{mod\to fuel,g} + R_{mod\to surfaces,g} \tag{35}$$

The probabilities corresponding to each of the terms on the right-hand side of Eq. (35) are obtained by dividing each term by the left-hand side of Eq. (35).

For determining the first term on the right-hand side of Eq. (35), the following detectors are defined in Serpent2 as follows:

- The thermal neutrons interacting in the moderator and that were thermal before the interaction are counted with a cell detector labelled detector 1 – “modtt”, whereas the thermal neutrons interacting in the moderator and that were fast before the interaction are counted with a cell detector labelled detector 2 – “modft”.
- The fast neutrons interacting in the moderator and that were fast before the interaction are counted with a cell detector labelled detector 3 – “modff”, whereras the fast neutrons interacting in the moderator and that were thermal before the interaction are counted with a cell detector labelled detector 4 – “modtf”.
- All fast neutrons interacting in the moderator are counted with a cell detector, labelled detector 5. Likewise, all thermal neutrons interacting in the moderator are counted with a cell detector, labelled detector 6.

For neutrons emitted from the moderator and interacting in the fuel region or crossing outer surfaces, sets of two detectors corresponding to either fast or thermal reaction rates, respectively, are used for each region other than the moderator region and for each outer surface. Counts in those detectors are recorded if the flag for detector 5 or detector 6 is set, and removed after interaction in those regions or after crossing those surfaces.

The above procedure could be simplified, as briefly explained hereafter. The simplification comes from the fact that tracking the energy of the incident neutrons is superfluous. Only neutrons scattered from the moderator, irrespective of their initial energy, need to be tracked. As a result, and taking as an illustrative example neutrons emitted from the moderator and first interacting in the moderator, detectors 5 and 6 can be combined, as well as detectors 1 and 2 together, and detectors 3 and 4 together. The same simplifications could be applied to neutrons emitted from the moderator and first interacting in the fuel region or escaping through the outer surfaces. This simplified procedure makes it easier to evaluate the required probabilities when more than two energy groups are considered. This simplified procedure was successfully tested in two energy groups.

Neutrons emitted from the fuel

The procedure described above cannot be applied to the neutrons emitted from the fuel. This is because neutrons emitted from the moderator are due to scattering reactions, for which detector flagging is kept after a scattering event. However, for neutrons emitted from the fuel by fission reactions, the flagging information from the parent neutron is not retained after the fission event. Another procedure is thus required, as detailed below.

Denoting as:

$N_{fuel,g}$: Neutrons in group g emitted from fuel
$R_{fuel\to fuel,g}$: Neutrons in group g emitted from fuel to first interact in fuel
$R_{fuel\to mod,g}$: Neutrons in group g emitted from fuel to first interact in moderator
$R_{fuel\to surfaces,g}$: Neutrons in group g emitted from fuel to escape through surfaces

(36)

the following relationship should be fulfilled:

$$N_{fuel,g} = R_{fuel\to fuel,g} + R_{fuel\to mod,g} + R_{fuel\to surfaces,g} \quad (37)$$

The probabilities corresponding to each of the terms on the right-hand side of Eq. (37) are obtained by dividing each term by the left-hand side of Eq. (37).

The neutron-induced interactions in the fuel region are caused by neutrons emitted from the fuel region, from the moderator region, or from the outer surfaces. Thus, the number of neutrons emitted from the fuel region and first interacting in the fuel region is determined by:

$$R_{fuel\to fuel,g} = R_{fuel,total,g} - \left(R_{mod\to fuel,g} + R_{surfaces\to fuel,g}\right) \quad (38)$$

where

$R_{fuel,total,g}$: Neutrons in group g having any kind of interaction in the fuel
$R_{mod\to fuel,g}$: Neutrons in group g emitted from moderator to first interact in fuel
$R_{surfaces\to fuel,g}$: Neutrons in group g entering from surfaces to first interact in fuel

(39)

The terms at the right hand side of Eq. (38) are determined using detectors defined in Serpent2 as follows:

- The total number of reactions in the fuel region is determined using one cell detector, labelled detector 1. Detector 1 thus determines the term $R_{fuel,total,g}$.
- A surface current detector, labelled detector 2, defined on the surface of the fuel region is used to flag all neutrons entering the fuel region.
- A cell detector, labelled detector 3, is used to count all reactions in the fuel region with the previous flag set, i.e. for neutrons entering the fuel region. Detector 3 thus determines the terms $R_{mod\to fuel,g} + R_{surfaces\to fuel,g}$.

Detectors 1 and 3 thus allow determining $R_{fuel\to fuel,g}$ according to Eq. (38).

An additional surface current detector, labelled detector 4, counting the number of neutrons crossing the fuel surface if the flag defined in detector 2 is *not* set, is also defined. Detector 4

excludes neutrons entering the surface of the fuel region, crossing the fuel region without interaction and leaving through the surface of the fuel region. Detector 4 thus counts the number of neutrons emitted from the fuel region. Several additional detectors are then defined so that they can be used to determine neutrons emitted from the fuel region (i.e. neutrons with flag set in detector 4) and either interacting in the moderator region (i.e. $R_{fuel \to mod,g}$) or crossing the outer surfaces (i.e. $R_{fuel \to surfaces,g}$).

Table 16 gives the maximum relative difference for the probabilities obtained between the method earlier developed (described in Section 4.2) and revised method presented above for the same test system as the one described in Section 4.1. The table also shows the significant reduction in computational time for the revised method as compared to the original method. The calculations with the original and revised methods were both performed with 2000 source neutrons per cycle, 500 active and 50 inactive cycles.

The dominant eigenvalue for the hybrid method based on the revised probabilities is 1.27014, whereas the reference Monte Carlo solution is 1.27007±0.00007$1.27007 \pm 0.00007$. The spatial distribution of the flux calculated remains unchanged between the original and revised methods to compute the probabilities in the hybrid method. This demonstrates that the revised method correctly computes the probabilities with a much lower computational cost.

Table 16 Comparison between the original method for evaluating the Monte Carlo probabilities (see Section 4.2) and the revised method.

Type of probabilities	Maximum relative difference in probabilities [%]	Computational time for the original method [min]	Computational time for the revised method [min]
Emitted from fuel	0.9	30	9
Emitted from moderator	0.3	44	6

Even if the number of detectors defined in the Serpent2 input files decreases significantly, as compared to the earlier method described in Section 4.2, different input files are used to estimate the probabilities for neutrons emitted from the fuel, for neutrons emitted from the moderator, and for neutrons emitted from the outer surfaces, respectively. Since many detectors need to be defined in Serpent2, splitting the calculation of the probabilities in three input files allows avoiding possible errors associated with the possible interdependence of so many detectors used for each case.

4.2 Description of the test system

Two configurations are solved. The first configuration is a single assembly containing 10x10 fuel pins and corresponds to the one already presented in Fig. 2. The second one corresponds

to 2x2 assemblies with 17x17 fuel pins per assembly and is represented in Fig. 6. Five kinds of fuel pins exist in the 2x2 configuration. The differences between the various fuel pins are only related to the enrichments of each kind of pin. The cladding and the gap are not modelled. Each fuel pin is thus only surrounded by moderator. The labelling of the pins (from one to six) is made according to the enrichment in U-235, with the fuel pin type one having the lowest enrichment.

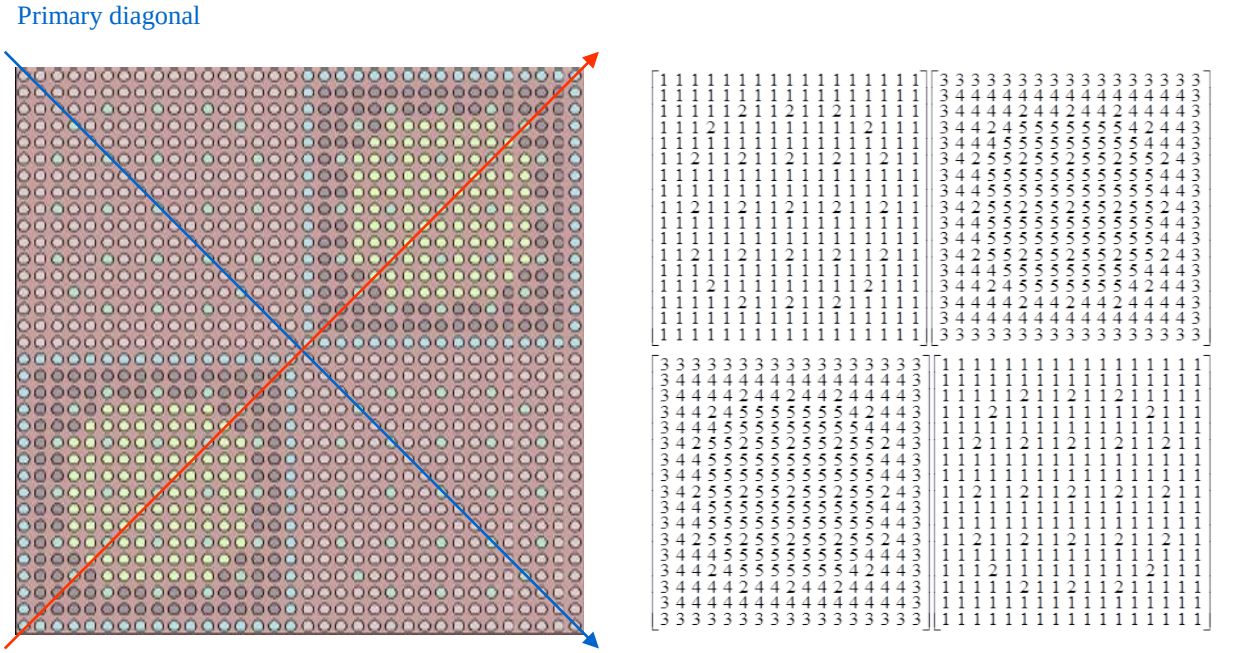

Fuel pin number	U-235 [1]	U-238 [1]	O-16 [1]
1	0.015867	0.86563	0.1185
2	0.018512	0.86299	0.1185
3	0.022919	0.85858	0.1185
4	0.026445	0.85505	0.1185
5	0.029971	0.85153	0.1185

Fig. 6 Radial layout of the modelled fuel assemblies (left) in the 2x2 configuration with the corresponding fuel pin types (right) and their respective compositions (mass fractions of materials in the fuel pins). The main and secondary diagonals along which the spatial distribution of the fluxes will be plotted are also indicated.

Both configurations are solved using pure Monte Carlo calculations (reference calculations) and using the hybrid method. In the latter case, the hybrid method relies on either 1x1 fuel pin cell/local problem (as represented in Fig. 3) or 2x2 fuel pin cells/local problem (as represented in Fig. 7). The revised procedure presented in Section 4.1 for estimating the probabilities can be easily extended to local systems made of more than 1x1 fuel cell.

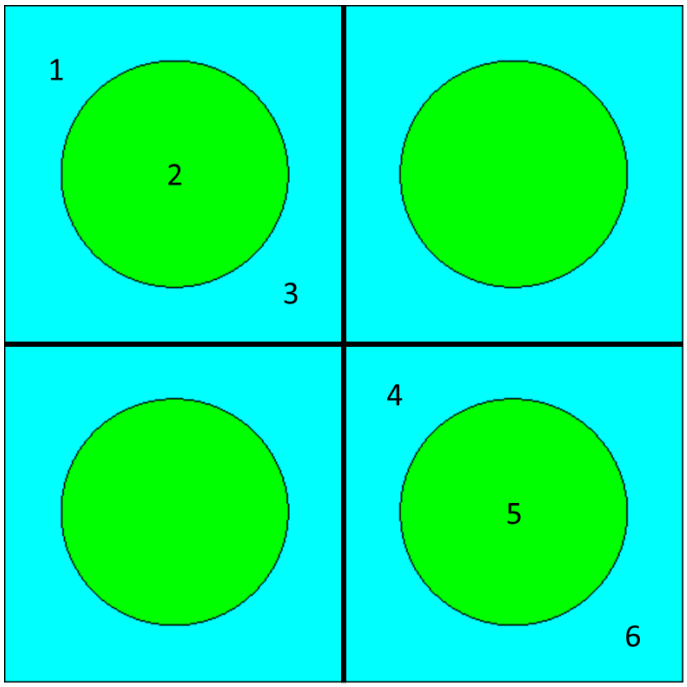

Fig. 7 Representation of an elementary subsystem (fuel region in green and coolant region in blue) made of 2x2 fuel pin cells. The numbers represent the labelling of the different regions later used to plot the variation of the flux along the diagonal.

4.3 Flux and eigenvalue calculations

The number of source neutrons per cycle (npop), the number of active cycles (cycles) and the number of inactive cycles (skip) used in the Monte Carlo calculations (for the reference Monte Carlo calculations and for the estimation of the probabilities required in the hybrid framework, respectively) are listed in Table 17.

Table 17 Computational set-up used in the Monte Carlo calculations.

	npop	cycles	skip
Monte Carlo reference calculations (one fuel assembly)	10000	5000	100
Monte Carlo reference calculations (2x2 fuel assemblies)	20000	5000	100
Monte Carlo probability calculations (1x1 fuel pin cell/local problem)	2000	500	50
Monte Carlo probability calculations (2x2 fuel pin cells/local problem)	4000	500	50

When using 1x1 fuel pin cell/local problem, the calculations of the probabilities have to be performed for each of the six fuel pin types. When using 2x2 fuel pin cells/local problem, the calculations have to be performed for the following combinations of the five fuel pin types:

$1{:}\begin{bmatrix}1 & 1\\ 1 & 1\end{bmatrix}$ $2{:}\begin{bmatrix}1 & 3\\ 1 & 3\end{bmatrix}$ $3{:}\begin{bmatrix}3 & 3\\ 4 & 4\end{bmatrix}$ $4{:}\begin{bmatrix}3 & 3\\ 4 & 3\end{bmatrix}$ $5{:}\begin{bmatrix}1 & 1\\ 1 & 2\end{bmatrix}$

$6{:}\begin{bmatrix}4 & 4\\ 4 & 4\end{bmatrix}$ $7{:}\begin{bmatrix}4 & 4\\ 2 & 4\end{bmatrix}$ $8{:}\begin{bmatrix}2 & 4\\ 5 & 5\end{bmatrix}$ $9{:}\begin{bmatrix}4 & 2\\ 5 & 5\end{bmatrix}$ $10{:}\begin{bmatrix}4 & 4\\ 5 & 5\end{bmatrix}$

$11{:}\begin{bmatrix}2 & 4\\ 5 & 4\end{bmatrix}$ $12{:}\begin{bmatrix}4 & 5\\ 5 & 5\end{bmatrix}$ $13{:}\begin{bmatrix}5 & 5\\ 2 & 5\end{bmatrix}$ $14{:}\begin{bmatrix}5 & 5\\ 5 & 5\end{bmatrix}$ $15{:}\begin{bmatrix}4 & 4\\ 5 & 2\end{bmatrix}$

$16{:}\begin{bmatrix}4 & 5\\ 2 & 4\end{bmatrix}$ $17{:}\begin{bmatrix}1 & 3\\ 3 & 1\end{bmatrix}$

All the other 2x2 combinations can be obtained by rotating the basic cells given above by 90 degrees clockwise, 90 degrees anticlockwise and 180 degrees (anti)clockwise. Such combinations thus do not require any new calculation of probabilities. As an illustrative example, the rotation of the 9th basic cell type given above gives the following patterns:

90 degrees clockwise: $\begin{bmatrix}5 & 4\\ 5 & 2\end{bmatrix}$

90 degrees anticlockwise: $\begin{bmatrix}2 & 5\\ 4 & 5\end{bmatrix}$

180 degrees (anti)clockwise: $\begin{bmatrix}5 & 5\\ 2 & 4\end{bmatrix}$

The computed eigenvalues for the 1x1 fuel assembly configuration and for the 2x2 fuel assembly configuration are reported in Table 18 and Table 19, respectively

Table 18 Evaluation of the dominant eigenvalue for the reference Monte Carlo solution and the hybrid solutions and for the 1x1 fuel assembly configuration.

Method	k_{eff}	$\Delta\rho \ \left[\mathrm{pcm}\right]$
Reference Monte Carlo solution	1.27007±0.00007	Reference
Hybrid solution (1x1 fuel pin cell/local problem)	1.27014	+7
Hybrid solution (2x2 fuel pin cell/local problem)	1.26975	-32

Table 19 Evaluation of the dominant eigenvalue for the reference Monte Carlo solution and the hybrid solutions and for the 2x2 fuel assembly configuration.

Method	k_{eff}	$\Delta\rho \ \left[\mathrm{pcm}\right]$
Reference Monte Carlo solution	1.20512±0.00005	Reference
Hybrid solution (1x1 fuel pin cell/local problem)	1.20950	+438
Hybrid solution (2x2 fuel pin cell/local problem)	1.20467	-45

In order to make the comparisons easier, the spatial distributions of the neutron fluxes along the diagonal through the modelled systems were normalized according to:

$$\sum_{i\in D}\frac{1}{k_{eff}}\left[\upsilon\Sigma_{f,1,i}\phi_{1,i}^{normalized}+\upsilon\Sigma_{f,2,i}\phi_{2,i}^{normalized}\right]=1 \qquad (40)$$

where the subscript i denotes the regions along the diagonal of the system being modelled containing along this diagonal D regions. An example of the labeling of the regions along the diagonal of the 2x2 fuel pin cells/local problem is for instance given in Fig. 7 as an illustrative example. Since the moderator for each fuel pin cell is treated as one region, the fluxes in node numbers 1 and 3 in that figure are identical. The same applies to the node numbers 4 and 6.

The spatial distributions of the fluxes for the hybrid solution and reference Monte Carlo solution and for the 1x1 fuel assembly configuration are given in Fig. 8 when using 1x1 fuel pin cell/local mesh and in Fig. 9 when using a 2x2 fuel pin cells/local mesh. The spatial distributions of the fluxes for the hybrid solution and reference Monte Carlo solution and for the 2x2 fuel assembly configuration are given in Fig. 10 when using 1x1 fuel pin cell/local mesh and in Fig. 11 when using a 2x2 fuel pin cells/local mesh along the primary diagonal. The spatial distributions of the fluxes for the hybrid solution and reference Monte Carlo solution and for the 2x2 fuel assembly configuration are given in Fig. 12 when using 1x1 fuel pin cell/local mesh and in Fig. 13 when using a 2x2 fuel pin cells/local mesh along the secondary diagonal.

For the 1x1 fuel assembly configuration, it can be seen from Table 18, Fig. 8 and Fig. 9 that the agreement between the hybrid solution and the reference Monte Carlo solution is very good for both 1x1 and 2x2 fuel pin cells/local mesh. The agreement in fast neutron flux is best for the 2x2 case, whereas the agreement is thermal neutron flux is best for the 1x1 case. The best agreement in the dominant eigenvalue is obtained for the 1x1 case. It should be observed that a slight difference in the buckling of the fast neutron flux is visible, as it was already noticed in Section 3.4.

For the 2x2 fuel assembly configuration, it can be seen from Table 18, Fig. 10, Fig. 11, Fig. 12 and Fig. 13 that the agreement between the hybrid solution and the reference Monte Carlo solution is much better for 2x2 fuel pin cells/local mesh compared to the 1x1 fuel pin cell/local mesh, except for the thermal neutron flux distribution along the secondary diagonal, where larger discrepancies are observed in the moderator region. The best agreement in the dominant eigenvalue is obtained for the 2x2 case. It is also observed that the buckling of the neutron flux is noticeably different in the hybrid framework.

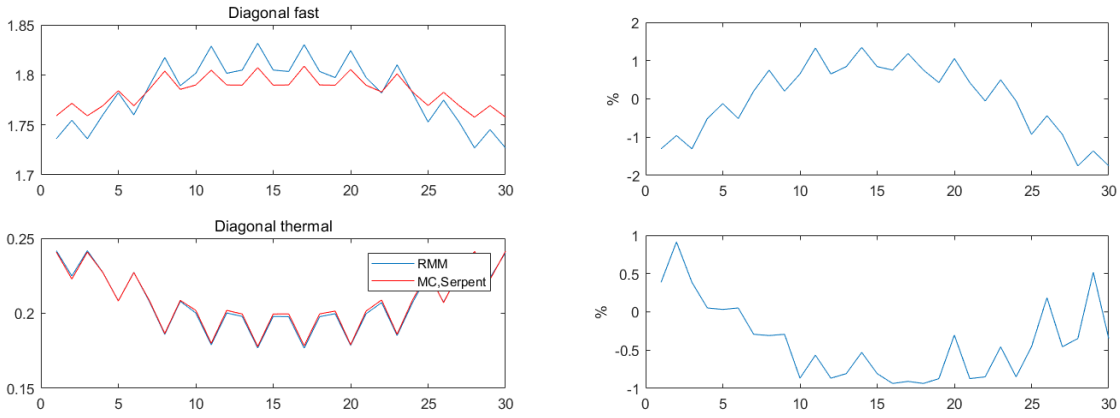

Fig. 8 Spatial distribution (left figures) and corresponding relative error (right figures) of the fast (top figures) and thermal (bottom figures) neutron fluxes along the diagonal of the 1x1 fuel assembly configuration for the reference Monte Carlo solution (in red, labelled as MC – Monte Carlo) and for the hybrid solution using the Monte Carlo probabilities (in blue, labelled as RMM – Response Matrix Method). The local problem in the hybrid modelling is made of 1x1 fuel pin cell.

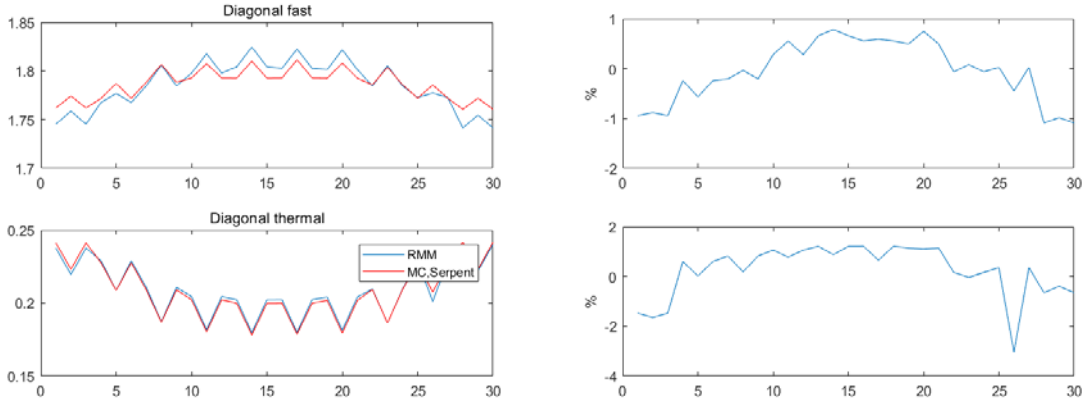

Fig. 9 Spatial distribution (left figures) and corresponding relative error (right figures) of the fast (top figures) and thermal (bottom figures) neutron fluxes along the diagonal of the 1x1 fuel assembly configuration for the reference Monte Carlo solution (in red, labelled as MC – Monte Carlo) and for the hybrid solution using the Monte Carlo probabilities (in blue, labelled as RMM – Response Matrix Method). The local problem in the hybrid modelling is made of 2x2 fuel pin cell.

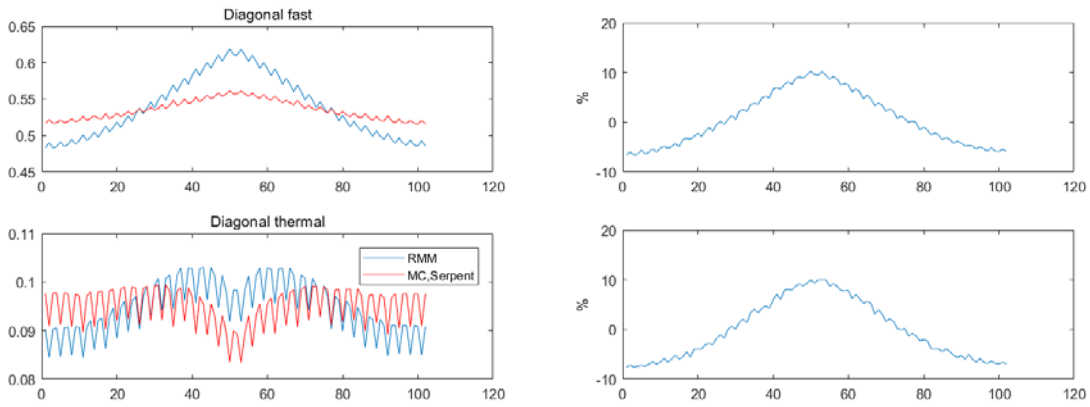

Fig. 10 Spatial distribution (left figures) and corresponding relative error (right figures) along the primary diagonal of the fast (top figures) and thermal (bottom figures) neutron fluxes along the diagonal of the 2x2 fuel assembly configuration for the reference Monte Carlo solution (in red, labelled as MC – Monte Carlo) and for the hybrid solution using the Monte Carlo probabilities (in blue, labelled as RMM – Response Matrix Method). The local problem in the hybrid modelling is made of 1x1 fuel pin cell.

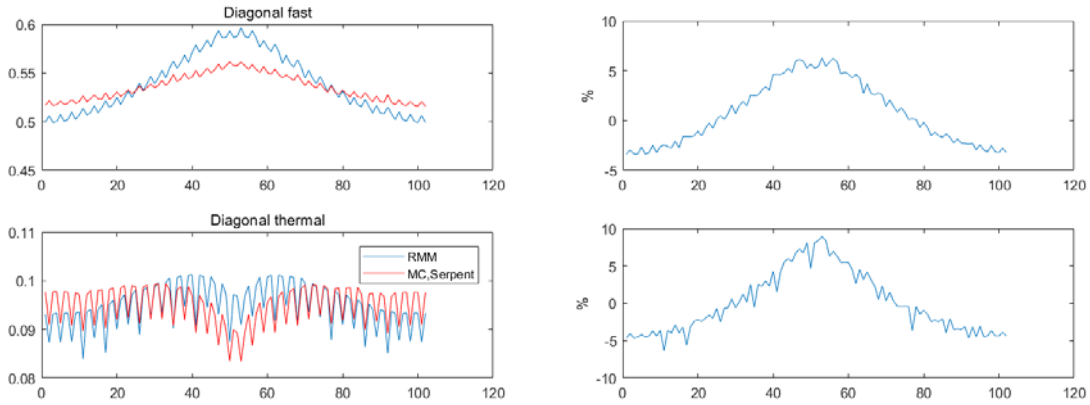

Fig. 11 Spatial distribution (left figures) and corresponding relative error (right figures) along the primary diagonal of the fast (top figures) and thermal (bottom figures) neutron fluxes along the diagonal of the 2x2 fuel assembly configuration for the reference Monte Carlo solution (in red, labelled as MC – Monte Carlo) and for the hybrid solution using the Monte Carlo probabilities (in blue, labelled as RMM – Response Matrix Method). The local problem in the hybrid modelling is made of 2x2 fuel pin cell.

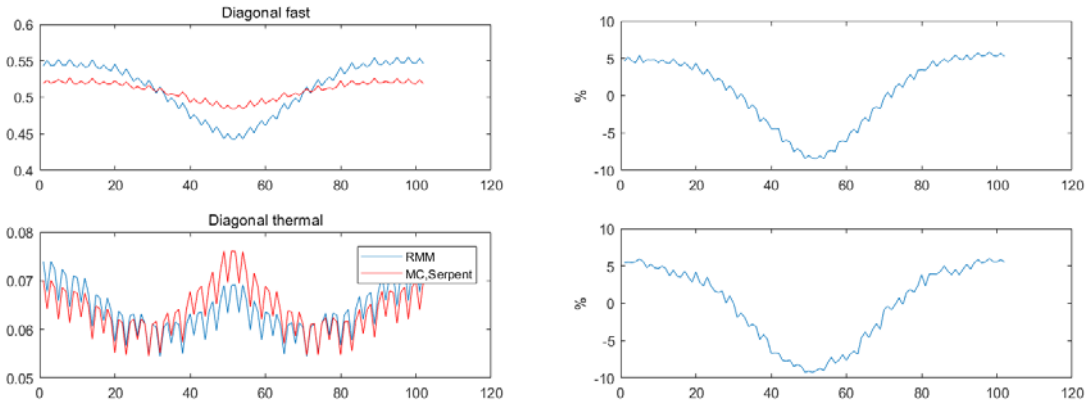

Fig. 12 Spatial distribution (left figures) and corresponding relative error (right figures) along the secondary diagonal of the fast (top figures) and thermal (bottom figures) neutron fluxes along the diagonal of the 2x2 fuel assembly configuration for the reference Monte Carlo solution (in red, labelled as MC – Monte Carlo) and for the hybrid solution using the Monte Carlo probabilities (in blue, labelled as RMM – Response Matrix Method). The local problem in the hybrid modelling is made of 1x1 fuel pin cell.

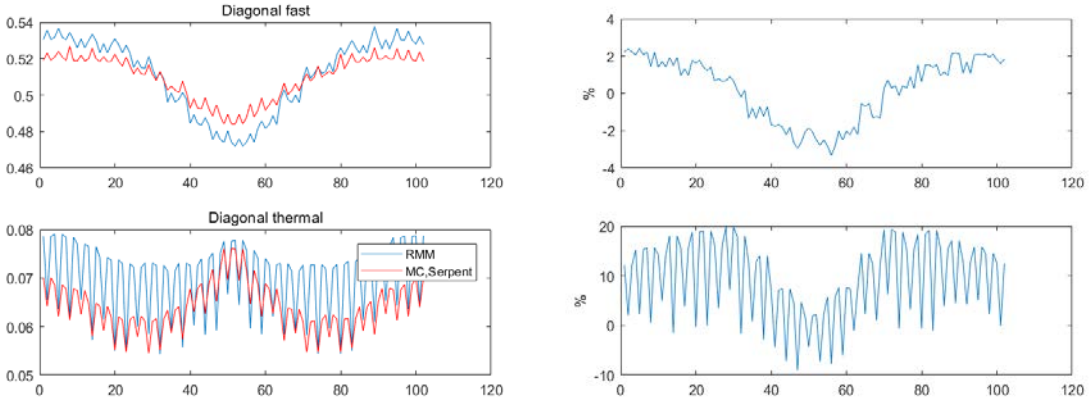

Fig. 13 Spatial distribution (left figures) and corresponding relative error (right figures) along the secondary diagonal of the fast (top figures) and thermal (bottom figures) neutron fluxes along the diagonal of the 2x2 fuel assembly configuration for the reference Monte Carlo solution (in red, labelled as MC – Monte Carlo) and for the hybrid solution using the Monte Carlo probabilities (in blue, labelled as RMM – Response Matrix Method). The local problem in the hybrid modelling is made of 2x2 fuel pin cell.

In order to identify the reason of the somewhat surprising higher discrepancies observed in the thermal neutron fluxes for the 2x2 fuel assembly configuration and the 2x2 fuel pin cells/local problem, some additional tests were performed. The local problem represented in Fig. 14 was thus considered. Two systems of 2x2 fuel pin cells were considered: the system earlier labelled one and made of four pin cells of type one, and the system earlier labelled four and made of three pin cells of type three and one pin cell of type four, i.e. the two considered system are:

$$1{:}\begin{bmatrix}1 & 1\\ 1 & 1\end{bmatrix} \text{ and } 4{:}\begin{bmatrix}3 & 3\\ 4 & 3\end{bmatrix}$$

The probabilities were estimated following the procedure earlier described. The ratio between the standard deviations of the detector counts used for evaluating the probabilities and the mean values of such detector counts are given in Table 20, for a few selected fuel pin types, a few detector counts, and the thermal group. It can be noticed that such ratios are very high, and in some cases much larger than unity. The reliability of the probabilities based on the above detector counts is thus highly questionable.

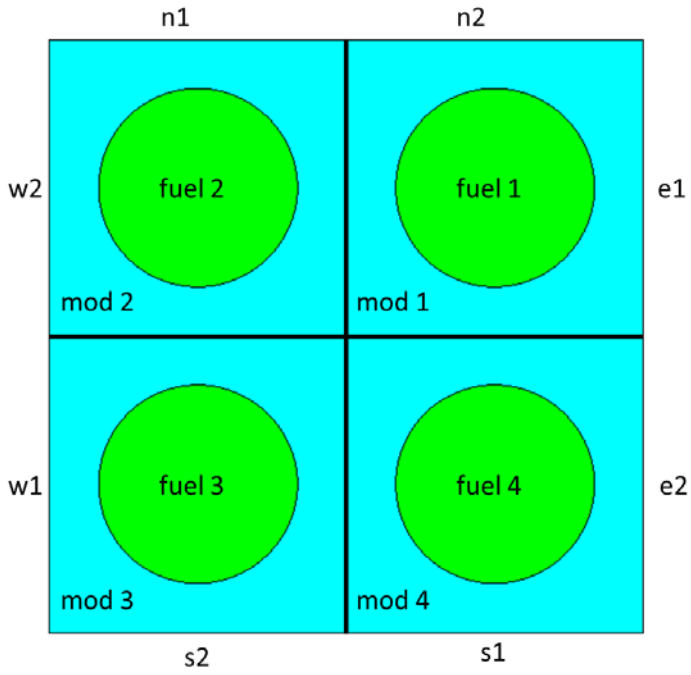

Fig. 14 Elementary 2x2 fuel pin cell system used for further testing. The labelling of the various regions and surfaces corresponds to the one for presenting the results in Table 20 and should not be mistaken with the types of fuel pins used.

Table 20 Ratio between the standard deviation and the mean values of some detector counts used in the estimation of some probabilities in the thermal group.

System type	$R_{fuel\ 1 \to mod\ 3}$	$R_{mod\ 1 \to fuel\ 3}$	$R_{mod\ 1 \to mod\ 3}$	$R_{mod\ 1 \to w2}$	$R_{w1 \to mod\ 1}$
1: $\begin{bmatrix} 1 & 1 \\ 1 & 1 \end{bmatrix}$	1.54	2.71	0.36	0.34	0.76
4: $\begin{bmatrix} 3 & 3 \\ 4 & 3 \end{bmatrix}$	2.69	3.28	0.5	0.53	1.3

A closer examination of some of the probabilities also revealed that the reciprocity relationship between probabilities is not always fulfilled. This occurs when the probabilities are expected to be very small. Following the procedure earlier explained, those probabilities are estimated to be equal to zero. Increasing the number of source neutrons from 4000 to 8000 and the number of active cycles from 500 to 1000 did not resolve this issue.

5 Conclusions and outlook

In this work, a hybrid neutron transport framework developed in the previous contract period was verified. The framework makes use of a deterministic approach relying on the response matrix method for which the required probabilities are estimated from the Monte Carlo Serpent2 code. For the deterministic calculations, a response matrix formulation combined with a power iteration technique was implemented in Matlab. New procedures were established for estimating the required probabilities in a more reliable manner and for decreasing the computational cost of the Monte Carlo calculations. The newly developed procedures can handle both 1x1 fuel pin cell and 2x2 fuel pin cells/local problem.

A benchmarking of the 1x1 probabilities against probabilities estimated "deterministically" demonstrated that the probabilities seem to qualitatively agree. The differences in the modelling assumptions used in the Monte Carlo and "deterministic" calculations of the probabilities might be the reason for not obtaining perfect quantitative agreement.

When using the hybrid framework on a single fuel assembly in an infinite lattice, the agreement between the hybrid solution and the Monte Carlo solution is very good. When applying the hybrid framework on a system of 2x2 fuel assemblies in an infinite lattice, the agreement somehow deteriorates, especially when only 1x1 fuel pin cell is used per local problem. Results drastically improve when 2x2 fuel pin cells are used, except for the thermal flux. 2x2 fuel pin cells/local problem might be more adequate to capture flux gradients existing between the pins in such local problems.

It should be mentioned that although the response matrix method used in the present framework relies on isotropic emissions in the laboratory reference system, the probabilities computed from Monte Carlo do not rely on such an approximation and should thus better describe the physics at hand.

The following points would need to be further investigated before considering larger systems and systems of larger dimensionality in the hybrid framework:

- The buckling of the fast neutron flux was systematically different from the reference solution. Since the mean free path of fast neutrons is much larger than for thermal neutrons, a tighter coupling on large scale exist. It should for instance be checked whether the calculations in Serpent2 include a criticality spectrum correction that might change the buckling of the neutron flux.
- A system that can be modelled for estimating the probabilities both deterministically and from Monte Carlo would need to be created. Using Carlvik's method, this would require that the outer boundary of the system is circular, and a white boundary condition is applied on the outer boundary. The latter cannot be presently modelled in Serpent2 (Leppänen, 2017).
- Some detectors counts were found to have bad statistics, thus rendering the associated probabilities less reliable. This seems to happen when the detector counts are very low. An automatic procedure that make use of the complementarity and reciprocity relationships the probabilities should fulfil should be developed, so that the probabilities having good statistics could be used for deducing the probabilities having otherwise poor statistics.
- When using more than one fuel pin cell per local problem, the spatial mesh needs to be internally refined in order to match the local problem. For instance, the 2x2 local mesh

considered in this work would most likely need to consider four azimuthal sectors per fuel pin in order to better treat the heterogeneous interactions between the four modelled fuel pins.

- The theoretical implications of the assumed isotropic emissions in the response matrix method needs to be further investigated, in particular considering the fact that no such approximation is made when estimating the probabilities from Monte Carlo. In addition, the development of a response matrix formulation for higher orders of the angular neutron flux than its first moments (scalar neutron flux and neutron currents) might be necessary.
- The effect of transport correcting the macroscopic cross-sections before being used in the hybrid framework should be assessed.
- The work performed by the Serpent2 code developers on the response matrix method for acceleration of the convergence of the fission source (Leppänen, 2018) should be studied and integrated in the present framework, if possible.

6 References

Carbol, S, Andersson, M, Demazière, C & Leppänen, J. 2017. Development of a hybrid neutron transport method in 2 energy groups. Report NKS-387, Nordic nuclear safety research, Roskilde, Denmark.

Carlvik, I. 1965. A method for calculating collision probabilities in general cylindrical geometry and application to the flux distributions and Dancoff factors. Proc. 3rd Int. Conf. Peaceful Uses of Atomic Energy, Geneva, Switzerland, August 31-September 9, 1964. A/CONF/28/P.681, Vol. 2, United Nations.

Demazière, C. 2013. Multi-physics modelling of nuclear reactors: current practices in a nutshell. International Journal of Nuclear Energy Science and Technology, 7 (4): 288–318.

Leppänen, J. 2017. Private communication.

Leppänen, J. 2018. Acceleration of fission source convergence in the Serpent 2 Monte Carlo code using a response matrix based solution for the initial source distribution. Proc. Int. Conf. Physics of Reactors – Reactor Physics paving the way towards more efficient systems (PHYSOR2018), Cancun, Mexico, April 22-26, 2018.

Leppänen, J, Pusa, M, Viitanen, T, Valtavirta, V & Kaltiaisenaho, T. 2015. The Serpent Monte Carlo code: Status, development and applications in 2013. Annals of Nuclear Energy. 82: 142 – 150.

Lux, I & Koblinger, L. 1991. Monte Carlo particle transport methods: neutron and photons calculations. CRC Press, Boca Raton, FL, USA.

Stacey, W M. 2001. Nuclear reactor physics. John Wiley & Sons, New York, NY, USA.

Stamm'ler, R J J & Abbate, M J. 1983. Methods of steady-state reactor physics in nuclear design. Academic Press, London, United Kingdom.

Bibliographic Data Sheet **NKS-413**

Title	Development of a hybrid neutron transport solver in 2 energy groups – final report
Author(s)	Huaiqian Yi, Christophe Demazière, Paolo Vinai and Jaakko Leppänen
Affiliation(s)	Chalmers University of Technology and Technical Research Centre of Finland (VTT)
ISBN	978-87-7893-502-1
Date	December 2018
Project	NKS- R / HYBRID
No. of pages	37
No. of tables	20
No. of illustrations	14
No. of references	9

Abstract
max. 2000 characters

This project investigates the feasibility of performing reactor physics calculations for nuclear cores using a hybrid neutron transport methodology, by combining deterministic and probabilistic modelling techniques. In the presented implementation, a deterministic response matrix method was developed in Matlab. The necessary probabilities appearing in the response matrix method were estimated in advance using a probabilistic solver – the Monte Carlo code Serpent2. Ultimately, the hybrid framework will combine the advantages of the deterministic approach (fast running calculations) with the ones of the probabilistic approach (high flexibility in modelling any geometry and high accuracy). In the response matrix method, two grids are used: one fine grid for estimating the scalar neutron flux and a coarse grid for computing the neutron currents on this grid. In this second phase of the project, the framework was verified and new procedures to estimate the required probabilities were developed. Several two-dimensional test cases were then developed for benchmarking the computation of such probabilities and for benchmarking the response matrix framework itself. Compared to the earlier phase of the project, the framework now provides very good results, with a deviation of the dominant eigenvalue smaller than typically 50 pcm.

Concerning the spatial distribution of the flux, some acceptable agreement was also obtained, with relative deviations generally smaller than 5%. In some cases, though, higher discrepancies were noticed. Additional investigations are necessary to identify the root cause of the larger observed deviations in such cases, in order to further increase the fidelity of the simulations.

Key words nuclear reactor calculations, neutron transport, deterministic methods, probabilistic methods, hybrid methods

---

Available on request from the NKS Secretariat, P.O.Box 49, DK-4000 Roskilde, Denmark.
Phone (+45) 4677 4041, e-mail nks@nks.org, www.nks.org